© 2024. Published by The Company of Biologists Ltd | Disease Models & Mechanisms (2024) 17, dmm050211. doi:10.1242/dmm.050211

RESEARCH ARTICLE

Conditional *in vivo* deletion of LYN kinase has little effect on a BRCA1 loss-of-function-associated mammary tumour model

Giusy Tornillo[1], Lauren Warrington[1], Howard Kendrick[1], Adam T. Higgins[1], Trevor Hay[1], Sam Beck[2] and Matthew J. Smalley[1,*]

ABSTRACT

LYN kinase is expressed in BRCA1 loss-of-function-dependent mouse mammary tumours, in the cells of origin of such tumours, and in human breast cancer. Suppressing LYN kinase activity in BRCA1-defective cell lines as well as in *in vitro* cultures of *Brca1*-null mouse mammary tumours is deleterious to their growth. Here, we examined the interaction between LYN kinase and BRCA1 loss-of-function in an *in vivo* mouse mammary tumour model, using conditional knockout *Brca1* and *Lyn* alleles. Comparison of *Brca1* tumour cohorts showed little difference in mammary tumour formation between animals that were wild type, heterozygous or homozygous for the conditional *Lyn* allele, although this was confounded by factors including incomplete *Lyn* recombination in some tumours. RNA-sequencing analysis demonstrated that tumours with high levels of *Lyn* gene expression had a slower doubling time, but this was not correlated with levels of LYN staining in tumour cells themselves. Rather, high *Lyn* expression and slower tumour growth were likely a result of B-cell infiltration. The multifaceted role of LYN indicates that it is likely to present difficulties as a therapeutic target in breast cancer.

KEY WORDS: BRCA1, LYN kinase, Cre-LoxP

INTRODUCTION

The protein product of the *BRCA1* gene is well established as a tumour suppressor, principally of breast and ovarian cancer (Fu et al., 2022; Molyneux et al., 2010). Women who inherit one functional and one mutated copy are at an approximately 70% lifetime risk of developing breast cancer and 40% lifetime risk of ovarian cancer (Kuchenbaecker et al., 2017). Tumour formation is associated with loss-of-heterozygosity events that delete the functional copy (Mahdavi et al., 2019) and is accelerated by concomitant inactivation of the TP53 (or p53) tumour suppressor protein (Kim et al., 2016; Liu et al., 2007; Zhu et al., 2022). However, carriers of *BRCA1* mutations may also show functional haploinsufficiency, which increases the risk of overt neoplasia (Lim et al., 2009).

The best-characterised role of BRCA1 is as a key component of error-free, homologous recombination-dependent repair of double-stranded DNA damage (Foo and Xia, 2022; O'Donovan and Livingston, 2010). The defect in this process in BRCA1 loss-of-function-associated cancer is exploited by the use of poly ADP-ribose polymerase (PARP) inhibitors for therapy (Mateo et al., 2019). However, BRCA1 has a number of additional functions not directly affecting DNA damage repair (although they may influence the process indirectly). These include acting as an E3 ubiquitin ligase, regulating transcription and control of centrosomal replication (Densham and Morris, 2017; Nolan et al., 2017; Yoshida and Miki, 2004).

The cells of origin of BRCA1-associated mammary tumours, the mammary luminal epithelial estrogen receptor (ESR1)-negative stem/progenitor population, express the c-KIT (or KIT) receptor tyrosine kinase at high levels, as well as its downstream pathway member, the SRC-family kinase LYN (Regan et al., 2012; Tornillo et al., 2018). LYN is overexpressed in human triple-negative breast cancer (TNBC; the breast cancer subtype most strongly associated with BRCA1 loss) (Choi et al., 2010; Croucher et al., 2013; Hochgrafe et al., 2010; Molyneux et al., 2010) and is also expressed at high levels in mammary tumours from *Brca1* conditional knockout mice (Molyneux et al., 2010). We have directly demonstrated using human breast cancer cell lines, primary cultures from *Brca1*-deleted mouse mammary tumours and cultures from human *BRCA1*-null patient-derived breast cancer xenografts that BRCA1 loss results in activation of LYN and downstream pathways, including the AKT pathway, and confers a growth and survival advantage to mammary tumour cells (Tornillo et al., 2018). We therefore suggested that *LYN* is an oncogene in the context of BRCA1 loss, and a potential therapeutic target in BRCA1 loss-of-function breast and ovarian cancers. However, this has not yet been tested in a gold-standard *in vivo* knockout mouse model. Therefore, we obtained a conditional knockout *Lyn* allele and crossed it to our established *BlgCre Brca1*$^{f/f}$ *p53*$^{+/-}$ mouse mammary tumour model. Surprisingly, we found that in this system, *BlgCre Brca1*$^{f/f}$ *p53*$^{+/-}$ mice carrying two conditional knockout *Lyn* alleles had a shorter overall survival than that of *BlgCre Brca1*$^{f/f}$ *p53*$^{+/-}$ mice heterozygous or wild type for *Lyn*, but there was no difference in mammary tumour-specific survival. Tumours with low levels of *Lyn* expression grew faster than tumours with high levels of *Lyn*; however, the extent of LYN protein expression in tumour cells as assessed by immunohistochemistry (IHC) was not correlated with tumour growth (although we were not able to assess LYN kinase activity in tumour cells). Rather, an increasing abundance of B cells in tumours was significantly associated with a slower tumour-doubling time. As B cells also express *Lyn*, this likely explained the correlation of tumour-doubling time with *Lyn* expression levels but not with LYN staining in tumour cells. Our

[1]The European Cancer Stem Cell Research Institute, School of Biosciences, Cardiff University, Cardiff CF24 4HQ, UK. [2]Independent Anatomic Pathology Ltd, Calyx House, South Road, Taunton TA1 3DU, UK.

*Author for correspondence (SmalleyMJ@cardiff.ac.uk)

H.K., 0000-0002-8685-3914; T.H., 0000-0003-1872-3971; M.J.S., 0000-0001-9540-1146

This is an Open Access article distributed under the terms of the Creative Commons Attribution License (https://creativecommons.org/licenses/by/4.0), which permits unrestricted use, distribution and reproduction in any medium provided that the original work is properly attributed.

Handling Editor: Elaine R. Mardis
Received 28 March 2023; Accepted 15 December 2023

Disease Models & Mechanisms (2024) 17, dmm050211. doi:10.1242/dmm.050211

results suggest that, as a therapeutic target in breast cancer, LYN kinase is likely to present difficulties.

RESULTS

The *Lyn*$^{fl(ex4)}$ allele is efficiently recombined *ex vivo*, resulting in loss of *Lyn* expression

We previously assessed the relationship between LYN and (*BRCA1*-associated) mammary tumourigenesis using, among other approaches, shRNA knockdown with two independent shRNA sequences (Tornillo et al., 2018). We controlled for off-target effects by re-expressing a *Lyn* cDNA that was resistant to the effects of the knockdown. Our findings suggested that functional LYN kinase was required for survival of BRCA1-null mammary tumour cells (Tornillo et al., 2018). However, the role of LYN in *BRCA1*-associated mammary tumourigenesis has not been investigated using the gold standard of conditional *in vivo* knockouts. Therefore, we obtained a mouse line carrying a conditional (floxed exon 4) *Lyn* allele (*Lyn*^{tm1c}; hereafter *Lyn*^{fl}) from the Mary Lyon Centre, Medical Research Council (MRC) Harwell, UK (Fig. 1A). Full details of these mice, the breeding strategies used to generate experimental cohorts and genotyping primers are provided in the Materials and Methods, Fig. S1 and Table S1.

We first used *Lyn*^{fl} mice to establish a cohort of animals in which expression of a tamoxifen-inducible Cre recombinase was driven from the ubiquitously active *Rosa26* promoter (hereafter *R26C*). This cohort also included a conditional floxed *Brca1* allele [*Brca1*$^{fl(ex22-24)}$; hereafter *Brca1*^{fl}] (McCarthy et al., 2007; Molyneux et al., 2010). To test the recombination of the *Lyn*^{fl} allele, mammary epithelial cells were harvested from *R26C Brca1*$^{fl/wt}$ *Lyn*$^{wt/wt}$, *R26C Brca1*$^{fl/wt}$ *Lyn*$^{fl/wt}$ or *R26C Brca1*$^{fl/wt}$ *Lyn*$^{fl/fl}$ mice and cultured as three-dimensional (3D) organoids according to our previous protocols (Tornillo et al., 2018). After 1 day, cultures were treated with 100 nM 4-hydroxytamoxifen (4OHT) or vehicle. After overnight incubation, cultures were washed to remove 4OHT and then cultured for a further 72 h prior to lysis for isolation of either RNA or protein. Quantitative real-time reverse-transcription PCR (qRT-PCR) analysis (Fig. 1B) demonstrated no difference in the expression of *Lyn* exon 4 among vehicle-treated *R26C Brca1*$^{fl/wt}$ *Lyn*$^{wt/wt}$, *R26C Brca1*$^{fl/wt}$ *Lyn*$^{fl/wt}$ or *R26C Brca1*$^{fl/wt}$ *Lyn*$^{fl/fl}$ cells, or between vehicle- and 4OHT-treated cells from *R26C Brca1*$^{fl/wt}$ *Lyn*$^{wt/wt}$ mice. However, there was a significant reduction in *Lyn* exon 4 expression levels in 4OHT-treated cells compared to those in vehicle-treated *R26C Brca1*$^{fl/wt}$ *Lyn*$^{fl/wt}$ cells, whereas *Lyn* exon 4 was undetectable in 4OHT-treated cells from *R26C Brca1*$^{fl/wt}$ *Lyn*$^{fl/fl}$

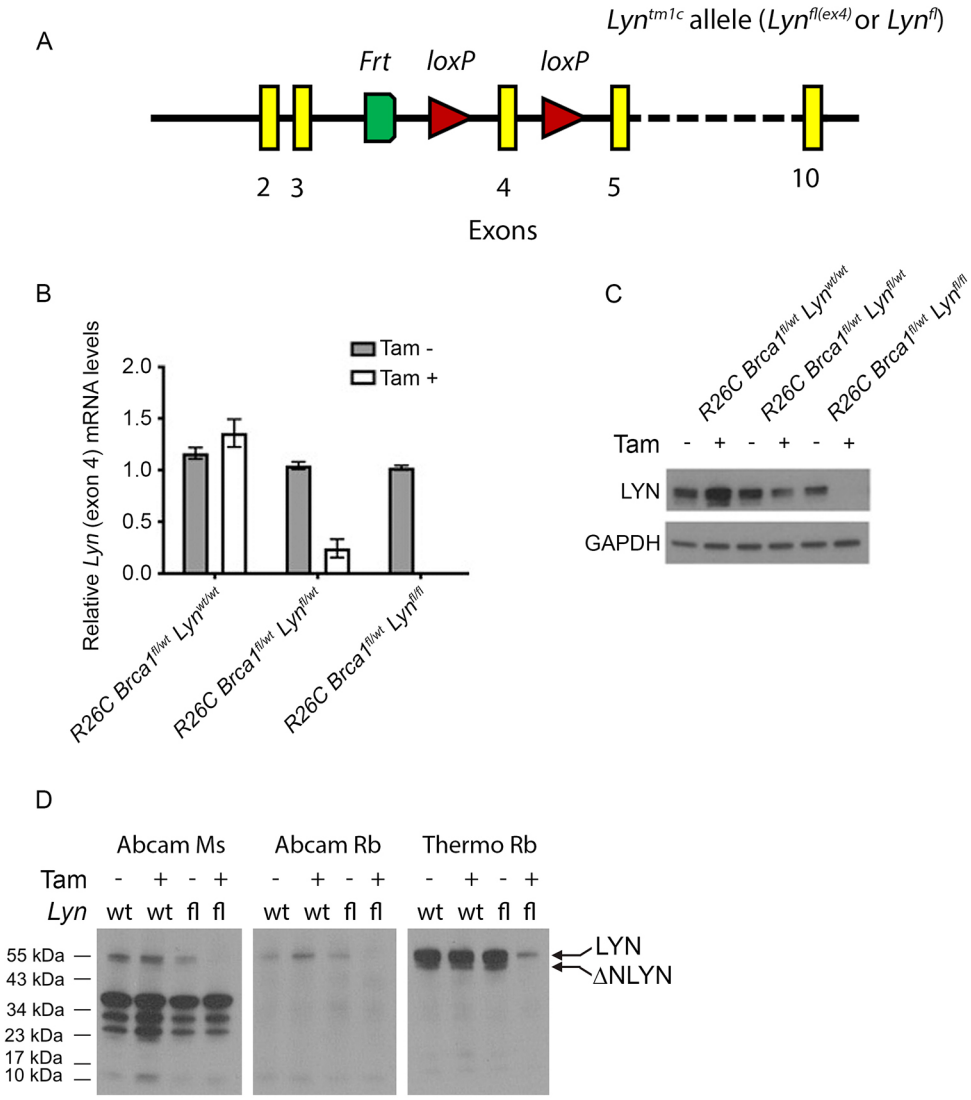

Fig. 1. The *Lyn*^{fl} allele is efficiently recombined *ex vivo* to deplete the LYN protein. (A) Schematic of the *Lyn*^{tm1c} [*Lyn*$^{fl(ex4)}$ or *Lyn*^{fl}] allele as supplied by the Mary Lyon Centre, MRC Harwell. The locations of *loxP* sites flanking exon 4 are indicated by red triangles. The single *Frt* site (green) is a remnant of the targeting strategy used to generate the allele. (B) qRT-PCR analysis of *Lyn* levels using an exon 4-specific probe in cultured primary mouse mammary epithelial cells from *R26C Brca1*$^{fl/wt}$ *Lyn*$^{wt/wt}$, *R26C Brca1*$^{fl/wt}$ *Lyn*$^{fl/wt}$ and *R26C Brca1*$^{fl/wt}$ *Lyn*$^{fl/fl}$ mice, treated with either vehicle control or tamoxifen (Tam). Mean±95% c.i. of exon 4 levels for the indicated condition relative to those for vehicle-treated *R26C Brca1*$^{fl/wt}$ *Lyn*$^{fl/wt}$ cells are shown (n=3 independent experiments, each using primary cells harvested from three mice of each genotype). (C) Western blot for LYN expression in representative protein extracts from the cell cultures analysed in B (using the Thermo Fisher Scientific polyclonal antibody against LYN). (D) Western blot analysis of LYN expression in *R26C Brca1*$^{fl/wt}$ *Lyn*$^{wt/wt}$ and *R26C Brca1*$^{fl/wt}$ *Lyn*$^{fl/fl}$ primary mammary epithelial cells, with or without tamoxifen treatment, using three different commercial anti-LYN antibodies. Each antibody was tested on identical loading of the same protein extracts (from a single cell preparation of each genotype). The expected LYN band and the putative ΔNLYN product visible with the Thermo Fisher Scientific rabbit polyclonal antibody are indicated. Ms, mouse; Rb, rabbit.

Disease Models & Mechanisms (2024) 17, dmm050211. doi:10.1242/dmm.050211

mice. Western blot analysis of protein extracts from these cultures (Fig. 1C) confirmed these results.

To provide further evidence that deletion of *Lyn* exon 4 results in a complete loss of LYN protein rather than, for example, generating a truncated protein that may have dominant-negative effects, protein lysates from *R26C Brca1*$^{fl/wt}$ *Lyn*$^{wt/wt}$ and *R26C Brca1*$^{fl/wt}$ *Lyn*$^{fl/fl}$ cells, treated with either vehicle or 4OHT, were analysed by western blotting using three different anti-LYN antibodies – a mouse monoclonal antibody (Abcam, ab1890) and two rabbit polyclonal antibodies (Abcam, ab32398; Thermo Fisher Scientific, PA5-81925) – in parallel (Fig. 1D; Table S1). In all other respects, the analysis was run identically, with identical amounts of protein loaded in all lanes. All three antibodies showed a substantial reduction in the amount of LYN protein detected in 4OHT-treated *R26C Brca1*$^{fl/wt}$ *Lyn*$^{fl/fl}$ cells, compared to that detected in other samples, and indeed, LYN was undetectable by the Abcam mouse monoclonal and rabbit polyclonal antibodies. The mouse monoclonal antibody generated a number of non-specific bands only observed with the other reagents in very over-exposed blots (see Fig. S8). The Abcam polyclonal antibody detected only a faint single band at the expected size, which disappeared in 4OHT-treatment of *Lyn*^{fl} cells. The Thermo Fisher Scientific rabbit polyclonal antibody detected a strong signal of the expected size, which was substantially reduced in the 4OHT-treated *R26C Brca1*$^{fl/wt}$ *Lyn*$^{fl/fl}$ sample, although a faint band was still visible, suggesting 100% recombination was not achieved in the cultures. The lower band visible with the Thermo Fisher Scientific polyclonal antibody was not an artefact associated with the *Lyn*^{fl} allele, as it was visible in extracts from both *Lyn*^{wt} and *Lyn*^{fl} cells. It was specific to LYN, as it disappeared upon 4OHT-treatment of *Lyn*^{fl} cells. It was not, however, the B isoform of LYN (hereafter LYNB) (Tornillo et al., 2018), as the A isoform (hereafter LYNA) and LYNB, were not fully resolved in the gradient gels used here (Tornillo et al., 2018). We hypothesize that the lower band is an endogenous product of caspase cleavage of LYN; a ΔNLYN variant has been previously described (Marchetti et al., 2009). Therefore, the *Lyn*^{fl} allele is recombined by Cre recombinase and, as a result, is unable to generate the protein.

A *BlgCre Brca1*$^{fl/fl}$ *p53*$^{+/-}$ *Lyn*$^{fl/fl}$ mouse cohort has reduced overall survival but few other differences compared to cohorts with wild-type *Lyn* alleles

Next, three cohorts of mice in which Cre expression was driven by the β-lactoglobulin promoter (*BlgCre*) were established. All three were homozygous for floxed *Brca1* alleles and also germline heterozygous for *Trp53* or *p53* (*BlgCre Brca1*$^{fl/fl}$ *p53*$^{+/-}$), similar to the lines that we previously used (McCarthy et al., 2007; Molyneux et al., 2010). One cohort was wild type for *Lyn* (*BlgCre Brca1*$^{fl/fl}$ *p53*$^{+/-}$ *Lyn*$^{wt/wt}$, *n*=19); in the second cohort, animals were heterozygous for the conditional *Lyn* allele (*BlgCre Brca1*$^{fl/fl}$ *p53*$^{+/-}$ *Lyn*$^{fl/wt}$, *n*=22); and in the third cohort, they were homozygous for the conditional *Lyn* allele (*BlgCre Brca1*$^{fl/fl}$ *p53*$^{+/-}$ *Lyn*$^{fl/fl}$, *n*=21). Mice were aged until defined humane endpoints were reached, at which point animals were euthanised and underwent a full necropsy. When mice developed mammary tumours, these were regularly measured to determine tumour-doubling times prior to the point at which euthanasia was necessary. Full details of all cohort animals and their pathology is provided in Tables S2 and S3.

We hypothesised that as LYN kinase activity was required for survival of cells that had lost BRCA1 activity (Tornillo et al., 2018), introducing the conditional *Lyn*$^{fl(ex4)}$ allele into the *BlgCre Brca1*$^{fl/fl}$ *p53*$^{+/-}$ background would result in a significant increase in overall survival (i.e. the age at which mice had to be euthanised for any reason) and also in mammary tumour-specific survival (i.e. the age at which mice had to be euthanised specifically as a result of the size of a mammary tumour). In contrast to our hypothesis, however, overall survival for *BlgCre Brca1*$^{fl/fl}$ *p53*$^{+/-}$ *Lyn*$^{fl/fl}$ mice was slightly, but significantly, shorter than that for *BlgCre Brca1*$^{fl/fl}$ *p53*$^{+/-}$ *Lyn*$^{fl/wt}$ mice (median survival of 350 days versus 365 days, respectively), although not significantly different to that for *BlgCre Brca1*$^{fl/fl}$ *p53*$^{+/-}$ *Lyn*$^{wt/wt}$ mice (median survival of 366 days) (Fig. 2A). There was no significant difference in mammary tumour-specific survival between the cohorts (Fig. 2B).

The majority of mice in all cohorts were euthanised because of the growth of the mammary tumours (Fig. 2C). Other reasons for euthanasia included scratches, vestibular syndrome or poor body condition score, with several examples of non-mammary neoplasia found upon necropsy, as well as reactive hyperplasia of the spleen. In seven cases, neoplastic epithelial deposits were observed in the lungs of animals carrying mammary tumours (Fig. S2A,B); in one of these cases, both the lung deposit and the primary tumour had a squamous histology, consistent with metastatic spread of the primary tumour (Fig. S2B). Other neoplastic lesions included haemangiosarcoma (one case) and osteosarcoma (two cases) (Fig. S2C-F). Histological analysis of enlarged spleens suggested that this was largely reactive but, in some cases, the histology was consistent with histiocytic sarcoma (two cases) or lymphoma (clonal analysis of B- and/or T-cell receptor rearrangement to confirm lymphoma was not carried out as this was not the primary focus of this study). Florid extra-medullary haematopoiesis was also noted in some cases. There was no visible difference in LYN staining in the white pulp of the spleen in *Lyn*$^{fl/fl}$ animals compared to that in other animals, with an expected decrease in LYN staining in proliferating B-cell germinal centres (Fig. S3).

There were no significant differences in the histotypes of mammary tumours between the cohorts (the majority of which were adenocarcinomas of no special type; Figs S4 and S5A). Many animals developed more than one tumour, and six of these developed more than one tumour in the same gland (Table S2), but there was no significant difference between the cohorts in terms of numbers of tumours developed by each animal (Fig. S5B). The growth of every mammary tumour that was palpable while an animal was alive was measured daily until a humane endpoint was reached. This enabled doubling times for every tumour with three or more measurements to be established. There was no significant difference in doubling times of mammary tumours between the cohorts (Fig. 2D). This was confirmed by Ki67 staining of sections from mammary tumours across the cohorts (considering only adenocarcinomas to eliminate different tumour histotypes as a potential confounding factor) (Fig. 2E; Table S4). Within each cohort there was, however, considerable heterogeneity in tumour-doubling times and, when animals that developed more than one tumour were considered individually, it was apparent that even in a single animal, doubling times of tumours could vary widely (Fig. 2F).

Cohort genotype only partly predicts LYN expression in tumours

Variation in the behaviour of tumours across a cohort, and indeed in multiple tumours from a single mouse, could result from partial floxed allele recombination in *Lyn*$^{fl/wt}$ or *Lyn*$^{fl/fl}$ mice, or from suppression of LYN expression by other mechanisms in *Lyn*$^{wt/wt}$ mice. If such variation existed, it would confound any analysis of

Disease Models & Mechanisms (2024) 17, dmm050211. doi:10.1242/dmm.050211

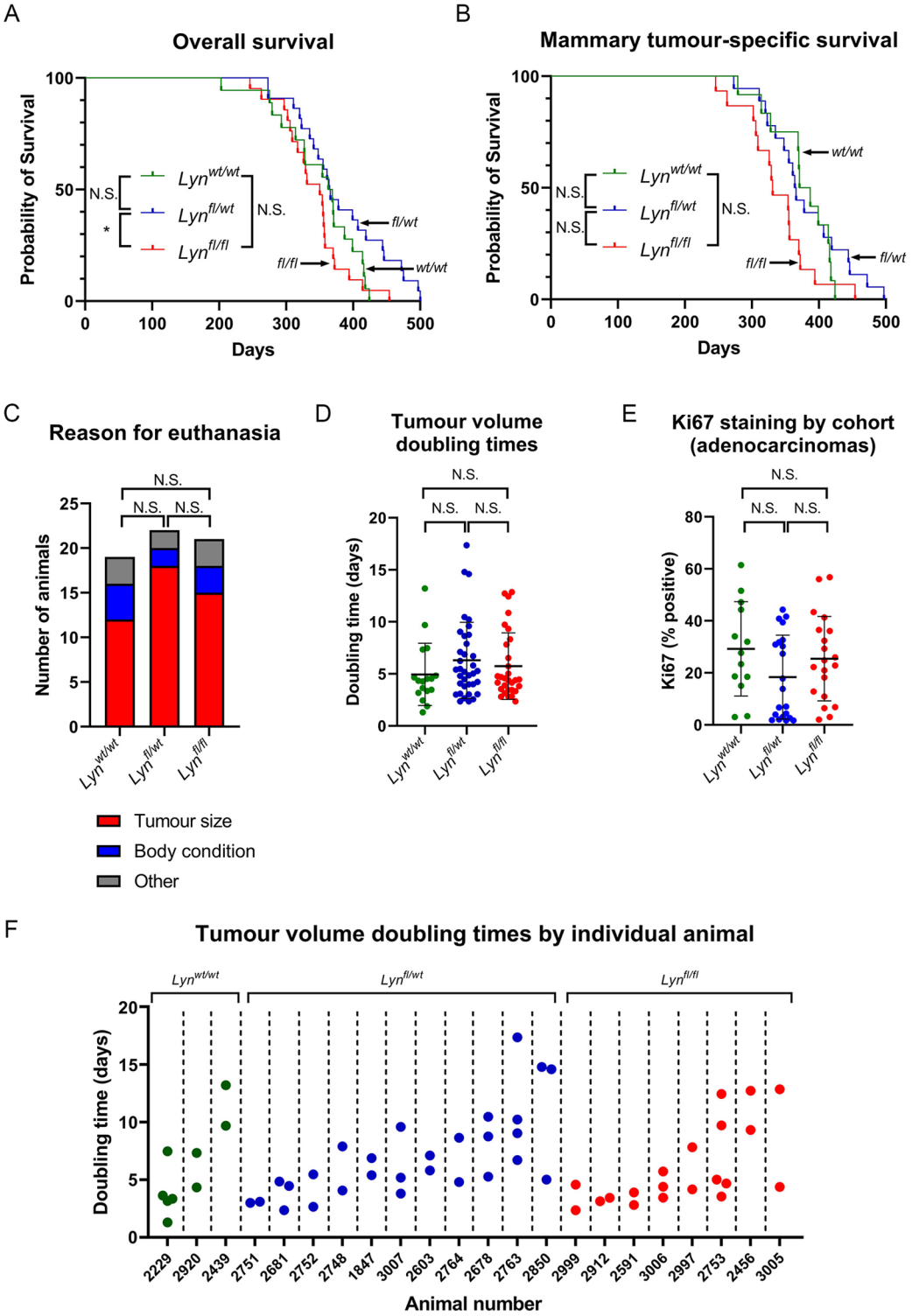

Fig. 2. *Lyn*$^{fl/fl}$ mice have decreased overall survival in the *BlgCre Brca1*$^{fl/fl}$ *p53*$^{+/-}$ model and have tumours with highly heterogeneous growth characteristics. (A) Kaplan–Meier curve of overall survival of *BlgCre Brca1*$^{fl/fl}$ *p53*$^{+/-}$ *Lyn*$^{wt/wt}$ (n=19), *BlgCre Brca1*$^{fl/fl}$ *p53*$^{+/-}$ *Lyn*$^{fl/wt}$ (n=22) and *BlgCre Brca1*$^{fl/fl}$ *p53*$^{+/-}$ *Lyn*$^{fl/fl}$ (n=21) cohorts. *Lyn*$^{fl/fl}$ mice had a significantly shorter survival than *Lyn*$^{fl/wt}$ mice (P<0.05; log rank test). (B) Kaplan–Meier curve of survival of *BlgCre Brca1*$^{fl/fl}$ *p53*$^{+/-}$ *Lyn*$^{wt/wt}$ (n=12), *BlgCre Brca1*$^{fl/fl}$ *p53*$^{+/-}$ *Lyn*$^{fl/wt}$ (n=18) and *BlgCre Brca1*$^{fl/fl}$ *p53*$^{+/-}$ *Lyn*$^{fl/fl}$ (n=15) cohorts considering only mice euthanised as a result of a mammary tumour reaching a specified endpoint. There were no significant differences (log rank test). (C) Reasons for euthanasia in *BlgCre Brca1*$^{fl/fl}$ *p53*$^{+/-}$ *Lyn*$^{wt/wt}$ (n=19), *BlgCre Brca1*$^{fl/fl}$ *p53*$^{+/-}$ *Lyn*$^{fl/wt}$ (n=22) and *BlgCre Brca1*$^{fl/fl}$ *p53*$^{+/-}$ *Lyn*$^{fl/fl}$ (n=21) cohorts. No significant differences were found (χ^2 test for trend). (D) Doubling times (days) for individual tumours in each cohort (n=17, 36, 30 for *Lyn*$^{wt/wt}$, *Lyn*$^{fl/wt}$ and *Lyn*$^{fl/fl}$, respectively). No significant differences (one-way ANOVA across cohorts; two-tailed unpaired t-tests comparing each cohort to the others). (E) Ki67 percentage positivity in sections of mammary adenocarcinomas from each cohort (n=13, 21, 20 for *Lyn*$^{wt/wt}$, *Lyn*$^{fl/wt}$ and *Lyn*$^{fl/fl}$, respectively). No significant differences were found (Kruskel–Wallis test across cohorts; Mann–Whitney test comparing each cohort to the others). In D,E, the value for each tumour is plotted with the mean±s.d. (F) Tumour volume doubling times (days) by animal showing only animals from each cohort with more than one tumour measured. N.S., not significant; *P<0.05.

Disease Models & Mechanisms (2024) 17, dmm050211. doi:10.1242/dmm.050211

the role of LYN in *Brca1*-dependent mammary tumourigenesis based solely on cohort genotype.

Therefore, to directly assess LYN expression levels in tumours from the three cohorts, 13 *Lyn*$^{wt/wt}$ tumours, 21 *Lyn*$^{fl/wt}$ tumours and 20 *Lyn*$^{fl/fl}$ tumours – all adenocarcinomas (no special type) – were randomly selected for staining for LYN protein (Fig. 3). LYN staining was assessed both qualitatively and semi-quantitatively using a histoscore approach based on the strength of staining and the area of the tumour stained (see Materials and Methods; Fig. S5C, Table S4). Scoring was carried out with the genotype masked; once scored, tumours were unmasked and analysed.

Staining patterns fell into three types: sheets and nests of epithelial-like tumour cells showing membrane staining (Fig. 3A); single cells scattered throughout the tumour, which were typically cells with pseudopodia and an appearance suggesting a motile phenotype (Fig. 3B, open arrowheads); and cells with the appearance of tumour-associated fibroblasts (Fig. 3B, black arrows).

Histoscore quantitation of LYN staining was carried out for the neoplastic epithelial-like tumour cells. LYN staining of these varied significantly with tumour genotype (Kruskal–Wallis test, P=0.0063) (Fig. 3C). There was a significant reduction in LYN staining in the cells of *Lyn*$^{fl/fl}$ tumours compared to that in *Lyn*$^{wt/wt}$ tumours (Mann–Whitney test, P=0.002) and *Lyn*$^{fl/wt}$ tumours (Mann–Whitney test, P=0.0344). However, some *Lyn*$^{fl/fl}$ tumours clearly retained strong LYN staining, whereas some *Lyn*$^{wt/wt}$ tumours showed very little or no staining. LYN staining in *Lyn*$^{fl/wt}$ tumours was reduced compared to that in *Lyn*$^{wt/wt}$ tumours but the difference was not statistically significant.

Although these results showed that, overall, there was a correlation between LYN staining of a tumour and the genotype of the animal the tumour came from, they also highlighted the variability in staining between tumours of the same genotype. This suggested that genotype could not be fully relied upon to predict LYN expression in any one individual tumour. To understand more objectively the relationship between tumour genotype and LYN expression in tumour cells, in the absence of cells from the tumour microenvironment that might also express LYN, we isolated live cells from six tumours of each cohort (*Lyn*$^{wt/wt}$, *Lyn*$^{fl/wt}$ and *Lyn*$^{fl/fl}$) and cultured them in conditions optimised for primary culture of epithelial tumour cells, before harvesting DNA, RNA and protein for analysis (DNA was only available for analysis from five of the six *Lyn*$^{fl/wt}$ samples).

Semi-quantitative PCR analysis of the *Lyn*^{fl} and *Lyn*^{wt} alleles demonstrated that the abundance of the *Lyn*^{wt} allele in primary cultures of *BlgCre Brca1*$^{fl/fl}$ *p53*$^{+/-}$ *Lyn*$^{fl/wt}$ tumours was approximately half that in cultures of *BlgCre Brca1*$^{fl/fl}$ *p53*$^{+/-}$ *Lyn*$^{wt/wt}$ tumours, as expected (Fig. 3D,E). However, there was also no significant difference overall in the abundance of the *Lyn*^{fl} allele between *BlgCre Brca1*$^{fl/fl}$ *p53*$^{+/-}$ *Lyn*$^{fl/wt}$ and *BlgCre Brca1*$^{fl/fl}$ *p53*$^{+/-}$ *Lyn*$^{fl/fl}$ tumour cells (Fig. 3D,F), and it is clear that although in some tumours, the *Lyn*^{fl} allele had recombined effectively, in others, it remained intact (Fig. 3D). Assessment of *Lyn* expression by qRT-PCR using a probe targeting exon 4 demonstrated that there was a significant reduction in *Lyn* expression in *BlgCre Brca1*$^{fl/fl}$ *p53*$^{+/-}$ *Lyn*$^{fl/fl}$ tumour cells compared to that in wild-type cells, but again, in some individual tumours, *Lyn* exon 4 expression was comparable to that seen in *Lyn*$^{wt/wt}$ tumours (Fig. 3G). *Brca1* expression was, as expected very low in tumours from all three lines relative to that in normal mammary epithelial cells (Fig. 3H), although not entirely absent, likely due to the presence of non-transformed, non-recombined epithelial cells derived from normal ducts trapped within the tumour and thus 'contaminating' the primary tumour cultures. Finally, assessment of LYN protein levels in these cells by western blotting showed that *Lyn*$^{fl/wt}$ tumour cells had significantly less protein than *Lyn*$^{wt/wt}$ tumour cells, but again, although some *Lyn*$^{fl/fl}$ tumour cells had low LYN protein levels, others had levels of LYN comparable to those in the wild-type cultures (Fig. 3I).

Transcriptional analysis of tumours demonstrates that tumours with high *Lyn* expression have a slower doubling time

Analysis of LYN protein levels in tumours demonstrated that although overall, there was a correlation between cohort genotype and LYN expression, there were a number of cases in which tumours from a *Lyn* wild-type mouse had very low or undetectable levels of LYN, whereas tumours from mice homozygous for the *Lyn* flox allele could actually have high levels of LYN expression. This, together with the presence of multiple tumours with different growth rates in some animals, confounded the analysis of the cohorts (Fig. 2A,B).

Therefore, to directly assess differences in the biology of the tumours from the cohorts, and to determine whether or not such differences were correlated with *Lyn* expression, we carried out an RNA-sequencing (RNAseq) analysis of tumour pieces from 39 tumours – 12 from *BlgCre Brca1*$^{fl/fl}$ *p53*$^{+/-}$ *Lyn*$^{wt/wt}$ mice, 14 from *BlgCre Brca1*$^{fl/fl}$ *p53*$^{+/-}$ *Lyn*$^{fl/wt}$ mice and 13 from *BlgCre Brca1*$^{fl/fl}$ *p53*$^{+/-}$ *Lyn*$^{fl/fl}$ mice. All were adenocarcinomas of no special type, to eliminate histological variation as a confounding factor. The sample details are provided in Table S5. The data were analysed in three ways, two of which were 'supervised' and one which was 'unsupervised'. First, significantly differentially expressed genes (DEGs) [adjusted P-value <0.05; ≤0.05 or ≥2.0 $\log_2$(fold change)] between tumours from *BlgCre Brca1*$^{fl/fl}$ *p53*$^{+/-}$ *Lyn*$^{wt/wt}$ and *BlgCre Brca1*$^{fl/fl}$ *p53*$^{+/-}$ *Lyn*$^{fl/fl}$ mice were identified (supervised analysis on the basis of genotype). Second, the normalised expression values for *Lyn* were used to rank the 39 tumour samples from those with the strongest *Lyn* expression to those with the weakest *Lyn* expression. Then, the 13 tumours most strongly expressing *Lyn* ('*Lyn*-high' group) were compared to the 13 tumours with the weakest *Lyn* expression ('*Lyn*-low' group) to identify DEGs (supervised analysis on the basis of *Lyn* expression). Finally, a principal component analysis (PCA) analysis was carried out on the complete normalised dataset of 39 tumours to identify any groups of tumours that could be distinguished from each other on the basis of transcriptional profiles in an unbiased manner. Significant DEGs were identified between the PCA groups (unsupervised analysis). The raw and normalised data for these comparisons are provided in Tables S6-S8. Significant DEGs are listed in Table S9, gene-set enrichment analysis (GSEA) using g:Profiler in Table S10 and a summary of enriched Gene Ontology Bioprocess (GO BP) and KEGG pathways in Table S11.

With the *BlgCre Brca1*$^{fl/fl}$ *p53*$^{+/-}$ *Lyn*$^{wt/wt}$ and *BlgCre Brca1*$^{fl/fl}$ *p53*$^{+/-}$ *Lyn*$^{fl/fl}$ comparison, only 93 significant DEGs were identified: 12 upregulated in *Lyn*$^{fl/fl}$ tumours relative to *Lyn*$^{wt/wt}$ tumours and 81 downregulated in *Lyn*$^{fl/fl}$ tumours relative to *Lyn*$^{wt/wt}$ tumours (Fig. 4A; Table S9). This emphasised our previous findings that animal genotype was not necessarily a good surrogate for *Lyn* expression or differences in tumour biology. Indeed, there was no difference in *Lyn* expression, as defined by normalised RNAseq *Lyn* counts, between the cohorts (Fig. 4B).

Next, we examined *Lyn* expression in all tumours as determined by the RNAseq data (ignoring genotypes) and compared this to

Disease Models & Mechanisms (2024) 17, dmm050211. doi:10.1242/dmm.050211

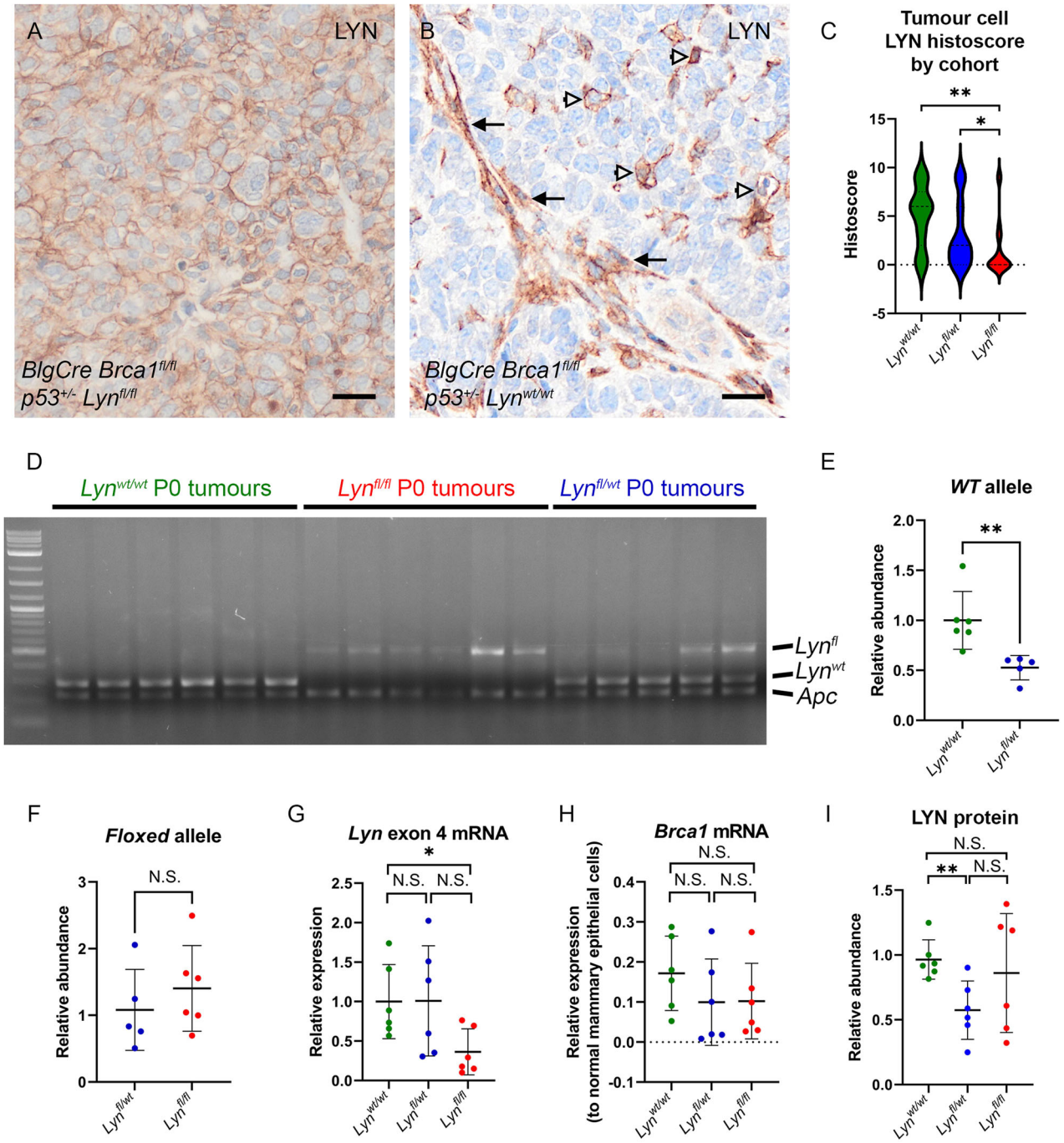

Fig. 3. LYN expression in tumours is heterogeneous but decreased overall in *BlgCre Brca1$^{fl/fl}$ p53$^{+/-}$ Lyn$^{fl/fl}$* mice. (A) LYN staining pattern in epithelial-like tumour cells. Scale bar: 20 µm. (B) LYN staining in single cells (open arrowheads) and cancer-associated fibroblast-like cells (black arrows). Scale bar: 20 µm. (C) 'Histoscore' quantitation of LYN staining in epithelial-like tumour cells (see Materials and Methods for details; *n*=13, 21 and 20 for *Lyn$^{wt/wt}$*, *Lyn$^{fl/wt}$* and *Lyn$^{fl/fl}$*, respectively). The *Lyn$^{fl/fl}$* cohort has significantly less staining than the *Lyn$^{wt/wt}$* or *Lyn$^{fl/wt}$* cohort (Mann–Whitney test). (D) Semi-quantitative PCR analysis of *Lyn$^{fl(ex4)}$* and *Lyn^{wt}* alleles in genomic DNA isolated from primary cultures of *BlgCre Brca1$^{fl/fl}$ p53$^{+/-}$ Lyn$^{wt/wt}$* (*n*=6), *BlgCre Brca1$^{fl/fl}$ p53$^{+/-}$ Lyn$^{fl/wt}$* (*n*=5) and *BlgCre Brca1$^{fl/fl}$ p53$^{+/-}$ Lyn$^{fl/fl}$* (*n*=6) tumour cells. Analysis of the *Apc* locus was included as a control to enable relative quantitation. Each PCR reaction included the primers for all three alleles. P0, passage 0/primary cultures. (E) Quantitation of the relative abundance of *Lyn^{wt}* alleles in D, considering only *Lyn$^{wt/wt}$* and *Lyn$^{fl/wt}$* cultures (as no *Lyn^{wt}* alleles were present in *Lyn$^{fl/fl}$* cells). There are 50% fewer (Mann–Whitney test) *Lyn^{wt}* alleles in the *Lyn$^{fl/wt}$* cultures compared to the *Lyn$^{wt/wt}$* cultures, as expected. (F) Quantitation of relative abundance of *Lyn$^{fl(ex4)}$* alleles in D, considering only *Lyn$^{fl/wt}$* and *Lyn$^{fl/fl}$* cultures (as no *Lyn^{fl}* alleles are present in *Lyn$^{wt/wt}$* cells). No significant difference was found between the samples, but the heterogeneity of the samples reflects the clear differences in band intensities seen in D. In E,F, data are presented as abundance in each sample relative to the *Apc* band in that sample. The mean abundance±s.d. of each group is indicated. (G) qRT-PCR analysis of *Lyn* exon 4 expression in primary tumour cell cultures. Data are presented as expression relative to the mean value for the *Lyn$^{wt/wt}$* cells (Mann–Whitney test). (H) qRT-PCR analysis of *Brca1* expression in primary tumour cell cultures. Data presented as expression relative to *Brca1* levels in lysates of freshly isolated normal mouse mammary epithelial cells for *Brca1* (Mann–Whitney test). (I) Relative expression of LYN protein in primary tumour cultures as determined by western blot analysis, quantified relative to standard loading controls and normalised to one *Lyn$^{wt/wt}$* tumour culture sample (Mann–Whitney test; see Fig. S8 for raw blots). For G-I, *n*=6 samples of each genotype; bars represent the mean±s.d. N.S., not significant; **P*<0.05; ***P*<0.01.

Disease Models & Mechanisms (2024) 17, dmm050211. doi:10.1242/dmm.050211

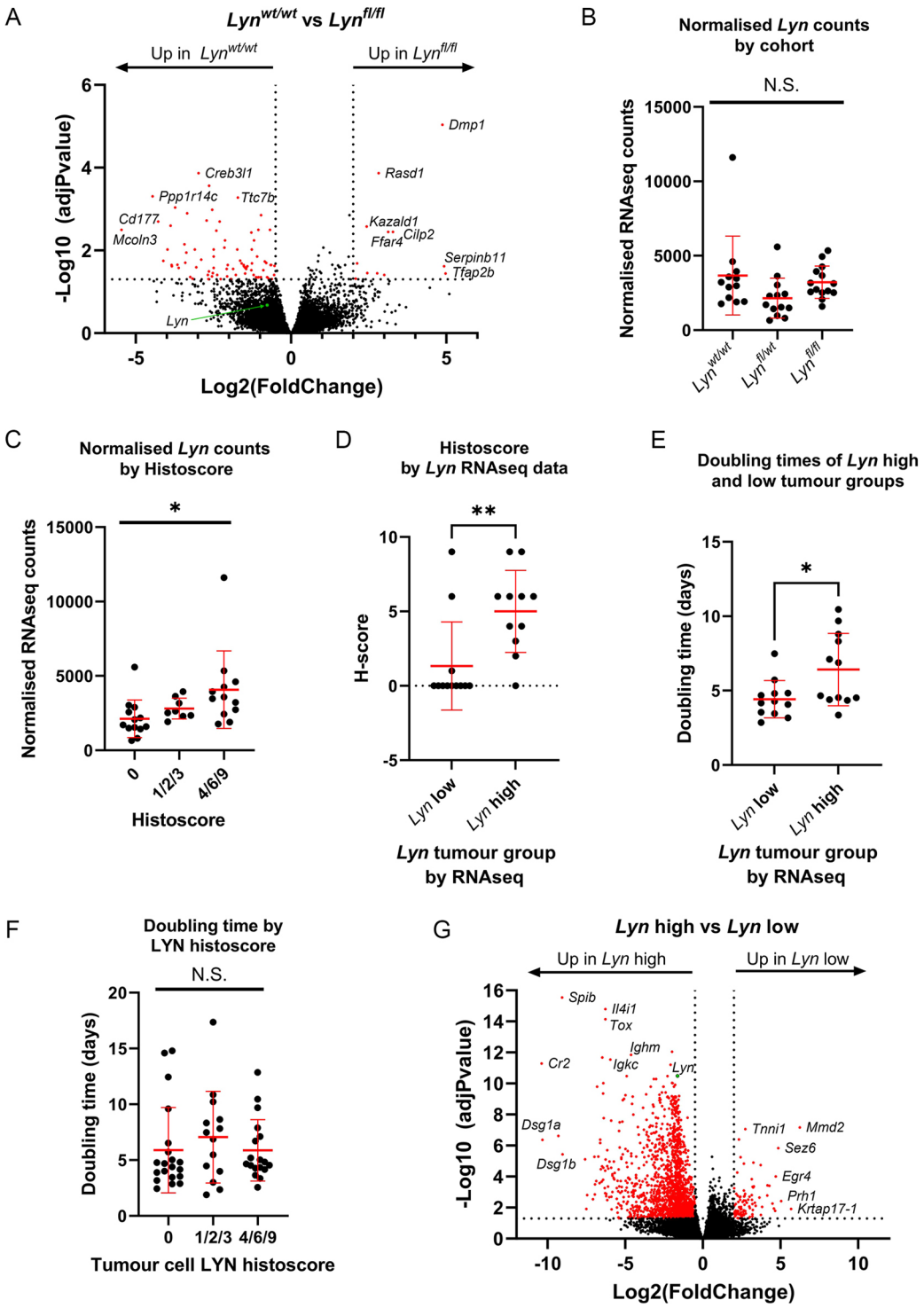

Fig. 4. Tumour molecular profiles correlate with *Lyn* expression but not with tumour cohort. (A) Volcano plot [$-\log_{10}$(adjusted *P*-value) against $\log_2$(fold change)] of DEGs comparing *Lyn*$^{wt/wt}$ (*n*=12) and *Lyn*$^{fl/fl}$ (*n*=14) tumours. Genes with an adjusted *P*-value of <0.05 and a fold change of ≤0.5 or ≥2 were considered significant and are indicated in red. The most strongly differentially expressed genes are labelled. *Lyn* is indicated with a green dot and labelled. (B) Normalised RNAseq *Lyn* counts in tumours from each cohort (*n*=12, 13 and 14 for *Lyn*$^{wt/wt}$, *Lyn*$^{fl/wt}$ and *Lyn*$^{fl/fl}$, respectively; Brown–Forsythe two-way ANOVA). (C) Normalised RNAseq *Lyn* counts in tumours with different LYN histoscore grading (0, no LYN staining; 1/2/3, low LYN staining or strong staining but only in a small region; 4/6/9, moderate to strong LYN staining) (*n*=13, 8 and 12, respectively). Increased *Lyn* counts are associated with increasing histoscore (Brown–Forsythe two-way ANOVA). (D) Histoscore of top tertile (*Lyn* high; *n*=12) versus bottom tertile (*Lyn* low; *n*=11) *Lyn*-expressing tumours by RNAseq (Mann–Whitney test). (E) *In vivo* doubling time (days) of top tertile (*Lyn* high; *n*=12) versus bottom tertile (*Lyn* low; *n*=12) *Lyn*-expressing tumours by RNAseq (two-tailed unpaired *t*-test). (F) *In vivo* doubling time (days) of tumours from LYN histoscore groups (*n*=20, 14 and 18, for groups 0, 1/2/3 and 4/6/9, respectively; Brown–Forsythe two-way ANOVA). (G) Volcano plot [$-\log_{10}$(adjusted *P*-value) against $\log_2$(fold change)] of DEGs comparing top tertile (*Lyn* high; *n*=13) versus bottom tertile (*Lyn* low; *n*=13) *Lyn*-expressing tumours defined by RNAseq. Genes with an adjusted *P*-value of <0.05 and a fold change of ≤0.5 or ≥2 were considered significant and are indicated in red. The most strongly differentially expressed genes are labelled. *Lyn* is indicated with a green dot and labelled. In B-F, mean±s.d. is shown. N.S., not significant; **P*<0.05; ***P*<0.01.

Disease Models & Mechanisms (2024) 17, dmm050211. doi:10.1242/dmm.050211

LYN staining (Table S4). Normalised *Lyn* counts were elevated in tumours with a LYN histoscore of 1/2/3 compared to tumours with a score of 0, and elevated further in 4/6/9-histoscore tumours compared to 1/2/3-scored tumours ($P<0.05$; two-way ANOVA; Fig. 4C). Consistent with this, when the tumours defined by normalised *Lyn* counts in the RNAseq as '*Lyn* high' and '*Lyn* low' (Table S5) were compared, the histoscore of the *Lyn*-high tumours was significantly greater than that of the *Lyn*-low tumours ($P<0.01$; Mann–Whitney test; Fig. 4D). There were, however, outliers showing that in some tumours, there was not a direct correlation between *Lyn* expression by RNAseq and LYN staining by IHC. We next compared the *in vivo* doubling time of the tumours defined as *Lyn* high and *Lyn* low (Fig. 4E) by RNAseq. *Lyn*-high tumours had a significantly longer doubling time ($P<0.05$; two-tailed unpaired *t*-test), suggesting that, in general, they grew more slowly than *Lyn*-low tumours and that they formed a distinct biological group. However, when the same tumours were divided into groups based on LYN histoscore of tumour cells, as directly assessed by IHC, there were no significant differences between tumours with no, moderate or high levels of LYN staining (Fig. 4F). Therefore, tumour-doubling time was correlated with *Lyn* expression in the tumours as a whole but not directly with LYN expression in the neoplastic cells.

There were 1655 DEGs significantly upregulated in *Lyn*-high relative to *Lyn*-low tumours and 100 DEGs significantly downregulated in *Lyn*-high relative to *Lyn*-low tumours (equivalent to 100 DEGs significantly upregulated in *Lyn*-low relative to *Lyn*-high tumours; Fig. 4G; Table S9). This number of DEGs, compared to the number identified when comparing by genotype, showed that categorising tumours by *Lyn* expression was better at defining sets of tumours with biologically meaningful differences than categorising tumours by the genotype of the cohort from which they were derived.

Finally, we used PCA analysis on the normalised RNAseq expression values for the whole tumour set to identify groups of tumours with similar gene expression patterns in an unbiased manner. This analysis initially suggested that the tumours could be split into either four groups (PCA groups 1, 2, 3 and 4; Fig. 5A) or two groups (combined groups 1/2 and 3/4). The normalised *Lyn* counts, LYN histoscores and *in vivo* tumour-doubling times were compared across either the four PCA groups individually or when combined into two groups (Fig. 5; Fig. S5D-F). Groups 3 and 4 had significantly elevated *Lyn* counts and a significantly higher LYN histoscore than groups 1 and 2 (Fig. S5D,E); the differences were more marked when comparing the combined group 3/4 against the combined group 1/2 (Fig. 5B,C). The combined group 3/4 had a significantly slower *in vivo* doubling time than the combined group 1/2 (Fig. 5D), but these differences were not significant in the four-group analysis (Fig. S5F). As the group 3 and 4 tumours appeared to behave similarly to each other, and the group 1 and 2 tumours also behaved similarly, the differences between the groups were more marked in the two-group analysis, the difference in doubling time suggested a real biological difference between groups 3/4 and 1/2, and the two-group approach enabled greater numbers of tumours to be compared in each group, we concentrated on the two-group approach and identified significant DEGs from PCA group 3/4 compared to PCA group 1/2. There were 835 DEGs significantly upregulated in PCA group 3/4 relative to PCA group 1/2 and 2437 DEGs significantly downregulated in PCA group 3/4 relative to PCA group 1/2 (equivalent to 2437 DEGs significantly upregulated in PCA group 1/2 relative to PCA group 3/4; Fig. 5E).

Considering that the PCA group 3/4 tumours had elevated *Lyn*/LYN expression (Fig. 5B,C), we next assessed the overlap between the sets of significant DEGs from the *BlgCre Brca1*$^{fl/fl}$ *p53*$^{+/-}$ *Lyn*$^{wt/wt}$ versus *BlgCre Brca1*$^{fl/fl}$ *p53*$^{+/-}$ *Lyn*$^{fl/fl}$ comparison, the *Lyn*-high versus *Lyn*-low tumour comparison and the PCA group 3/4 versus PCA group 1/2 comparison, using Venny (https://bioinfogp.cnb.csic.es/tools/venny/) (Fig. 5F). There was very little overlap between the *BlgCre Brca1*$^{fl/fl}$ *p53*$^{+/-}$ *Lyn*$^{wt/wt}$ versus *BlgCre Brca1*$^{fl/fl}$ *p53*$^{+/-}$ *Lyn*$^{fl/fl}$ DEGs and the other comparisons. However, 340 genes were identified as significantly differentially expressed in both the *Lyn*-high versus *Lyn*-low comparison and the PCA group 3/4 versus PCA group 1/2 comparison. Of these, 282 were upregulated in both *Lyn*-high and PCA group 3/4 tumours, whereas 57 were upregulated in both *Lyn*-low and PCA group 1/2 tumours. Only one gene was elevated in *Lyn* high and PCA group 1/2 tumours (Table S10).

The distribution of the *Lyn*-high and *Lyn*-low tumours within the PCA groups was consistent with these results. Of the PCA group 3/4 tumours, six were also in the *Lyn*-high tumour group, whereas four were tumours with intermediate *Lyn* expression. There were no *Lyn*-low tumours in PCA group 3/4. PCA group 1/2 included all the *Lyn*-low tumours, nine tumours with intermediate *Lyn* expression and seven *Lyn*-high tumours. Notably, the *Lyn*-high tumours in PCA group 3/4 were six of the seven tumours with the highest rank for *Lyn* expression by RNAseq, the one exception being one of the *Lyn*-high tumours in PCA group 1/2 that ranked second in *Lyn* expression by RNAseq but had been scored 0 for LYN expression by IHC (Table S5).

Lyn-high and PCA group 3/4 tumours are enriched in inflammatory signalling pathways, whereas PCA group 1/2 tumours are enriched in morphogenesis and cancer-associated signalling pathways

We next performed GSEA of the DEGs from the *Lyn*-high versus *Lyn*-low and the PCA group comparisons using g:Profiler. Genes significantly differentially expressed in the two comparisons were annotated separately and then overlaps between the annotations assessed. Full details are provided in Table S10. For ease of interpretation, we concentrated on understanding differentially enriched GO BP terms and KEGG pathways. GO BP terms were grouped by functional categories to facilitate this. The GO BP and KEGG analysis is summarised in Table S11 and Fig. 6.

Lyn-high tumours were enriched for 48 GO BP terms and 17 KEGG pathways. *Lyn*-low tumours were enriched for three GO BP terms but no KEGG pathways. PCA group 1/2 tumours were enriched for 477 GO BP terms and 14 KEGG pathways, whereas PCA group 3/4 tumours were enriched for 48 terms and 17 KEGG pathways (Table S11). The overlaps in GO BP and KEGG pathways between the tumour groups was striking and reflected the overlap seen in the DEGs. The list of enriched GO BP and KEGG pathways in the *Lyn*-high and PCA group 3/4 tumours was identical. Seven of these GO BPs were also enriched in PCA group 1/2; however, the majority (469 out of 477) of GO BP terms and all KEGG terms enriched in PCA group 1/2 were not found in the other groups (Fig. 6A,B).

GO BP terms were categorised into functional classes (Table S11) and the proportions of enriched terms from each functional class assessed for the tumour groups (Fig. 6C). Unsurprisingly, given that the terms enriched in the *Lyn*-high and PCA group 3/4 tumours were identical, the classification of GO BP terms in these groups was identical. For both of these sets,

Disease Models & Mechanisms (2024) 17, dmm050211. doi:10.1242/dmm.050211

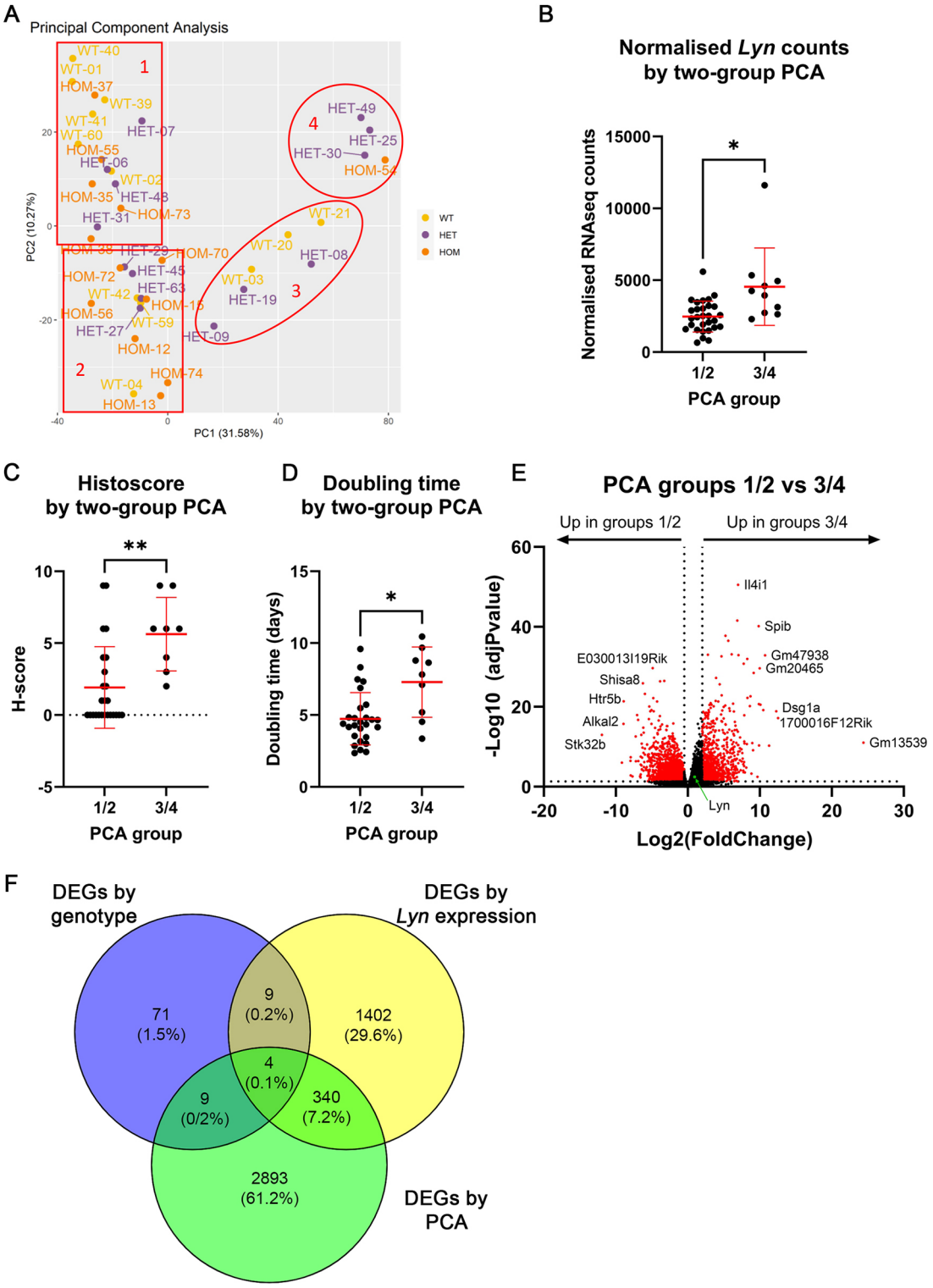

Fig. 5. PCA identifies two main groups of tumours that partially overlap with *Lyn*-high and *Lyn*-low tumours. (A) PCA plot of 39 tumours analysed by RNAseq showing an unbiased assessment of tumour gene expression differences and similarities. Principal component (PC) 1 (PC1) divides the tumours into groups 1/2 (n=29) and 3/4 (n=10), PC2 further divides the tumours to give four groups; however, the majority of the differences between the tumour groups was generated by PC1. WT, wild-type tumours; HET, heterozygous tumours; HOM, homozygous tumours. (B) Normalised RNAseq *Lyn* counts in tumours from PCA groups 1/2 (n=29) and 3/4 (n=10) (two-tailed unpaired *t*-test). (C) Histoscore of tumours from PCA groups 1/2 and 3/4 (Mann–Whitney test). (D) *In vivo* doubling time (days) of tumours from PCA groups 1/2 (n=27) and 3/4 (n=9) (two-tailed unpaired *t*-test). (E) Volcano plot [$-\log_{10}$(adjusted *P*-value) against $\log_2$(fold change)] of DEGs comparing tumours from PCA groups 1/2 (n=29) and 3/4 (n=10). Genes with an adjusted *P*-value of <0.05 and a fold change of ≤0.5 or ≥2 were considered significant and are indicated in red. The most strongly differentially expressed genes are labelled. *Lyn* is indicated with a green dot and labelled. (F) Venn diagram showing overlap between DEGs identified when comparing $Lyn^{wt/wt}$ versus $Lyn^{fl/fl}$ tumours, *Lyn*-high versus *Lyn*-low tumours and PCA group 1/2 versus PCA group 3/4 tumours. Note that 340 genes overlap between the latter two groups, but there is very little overlap with the $Lyn^{wt/wt}$ versus $Lyn^{fl/fl}$ tumour data. In B-D, mean±s.d. is shown. **P*<0.05; ***P*<0.01.

Disease Models & Mechanisms (2024) 17, dmm050211. doi:10.1242/dmm.050211

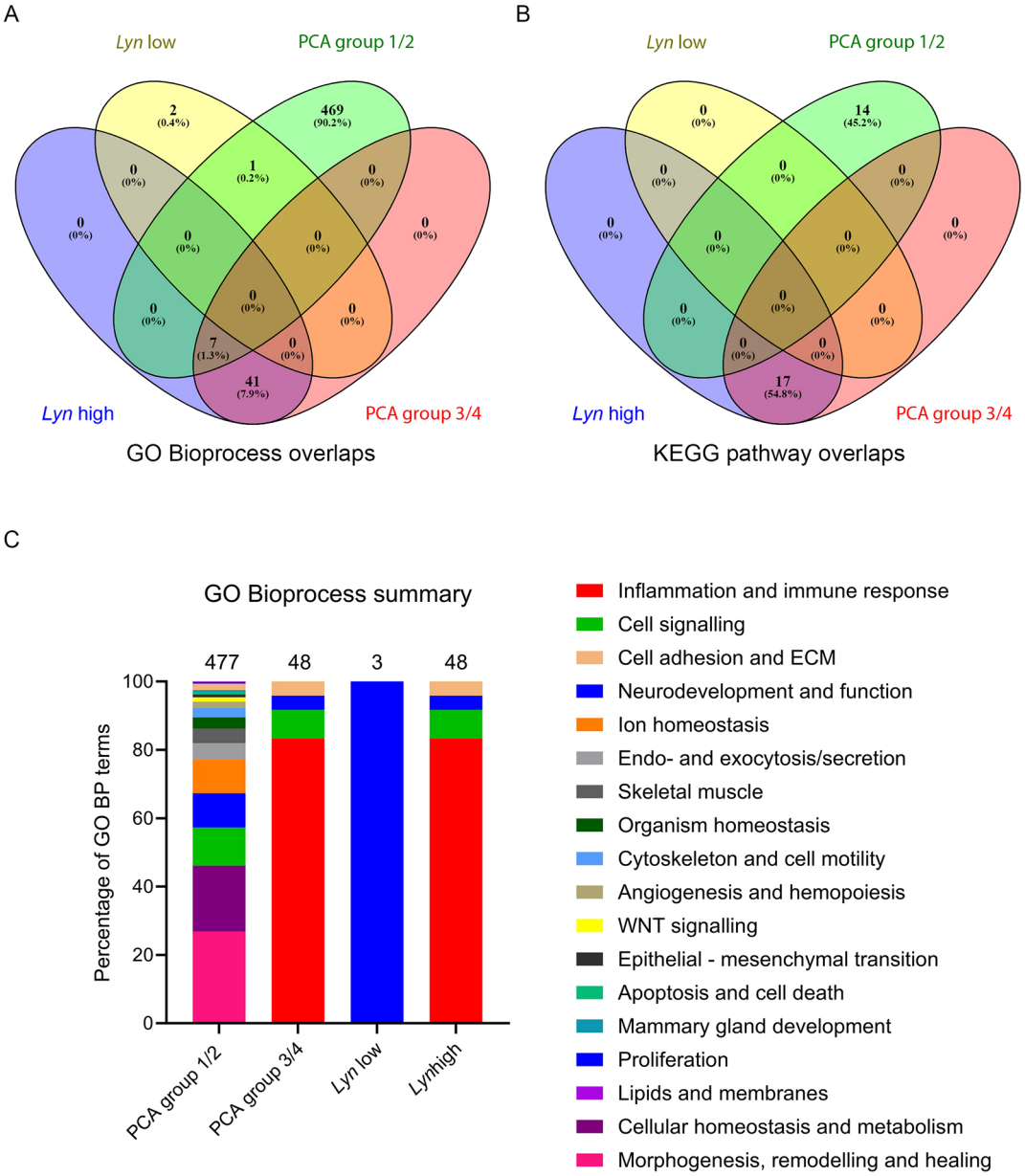

Fig. 6. The *Lyn*-high and PCA group 3/4 tumours are enriched for identical biological functions. (A,B) Venn diagram analysis of overlap between Gene Ontology Bioprocess (GO BP) terms (A) and between KEGG pathways (B) enriched in the DEGs from *Lyn*-high, *Lyn*-low, PCA group 1/2 and PCA group 3/4 tumours. (C) Distribution of enriched GO BP terms within functional categories for the *Lyn*-high, *Lyn*-low, PCA group 1/2 and PCA group 3/4 tumours. The number of enriched GO BP terms identified in the DEGs of each tumour group is indicated above each bar. Each bar is divided according to the percentage of enriched GO BP terms falling into each functional category (indicated by the colour key).

the most numerous classification of enriched GO BP terms was ‘inflammation and immune response’ (40 terms, 83.3%), followed by ‘cell signalling’ (four terms, 8.3%), ‘cell adhesion and extracellular matrix (ECM)’ (two terms, 4.2%) and ‘neurodevelopment and function’ (two terms, 4.2%). For the *Lyn*-low tumours, the three enriched GO BP terms were all classified as associated with ‘neurodevelopment and function’ (100%). The 477 GO BP terms enriched in PCA group 1/2 could be classified into 17 different functional classes. The four largest of these (to which >10% of the 477 GO BP terms were assigned) were ‘morphogenesis, remodelling and healing’ (128 terms, 26.8%), ‘cellular homeostasis and metabolism’ (92 terms, 19.3%), ‘cell signalling’ (53 terms, 11.1%) and ‘neurodevelopment and function’ (48 terms, 10.1%).

We next examined the enriched KEGG pathways. Consistent with the GO BP analysis, and the overlap of the annotations between the tumour groups, the *Lyn*’high/PCA group 3/4 tumours were enriched for KEGG pathways including ‘cytokine-cytokine receptor interaction’, ‘NFκB signalling’, ‘chemokine signalling’, ‘TNF signalling pathway’ and ‘apoptosis’. In contrast, the PCA group 1/2 tumours were enriched for KEGG pathways including ‘breast cancer’, ‘Wnt signalling’, ‘Notch signalling’, ‘PI3K-Akt signalling’ and ‘pathways in cancer’ (Table S11).

In vivo differences between tumour groups are not maintained in cultured neoplastic cells

We next carried out qRT-PCR analysis of expression of seven ‘inflammation and immunity’-/‘NFκB’-associated genes (*Bcl2a1a*,

Disease Models & Mechanisms (2024) 17, dmm050211. doi:10.1242/dmm.050211

Cd40, *Nfkb2*, *Relb*, *Ccl5*, *Tnfaip3* and *Shisa8*) differentially expressed between the *Lyn* groups and PCA groups of tumours using twenty of the samples (Table S12) analysed by RNAseq in order to validate the analysis. The results confirmed that the genes were significantly differentially expressed between the *Lyn*-low and *Lyn*-high (Fig. 7A; Table S12; Fig. S7) and between the PCA group 1/2 and PCA group 3/4 tumour groups (Fig. 7B) and in expected patterns (*Bcl2a1a*, *Cd40*, *Nfkb2*, *Relb*, *Il4i1*, *Ccl5* and *Tnfaip3* were significantly more highly expressed in *Lyn*-high and PCA group 3/4 tumours, *Shisa8* was significantly more highly expressed in *Lyn*-low and PCA group 1/2 tumours).

Then, we analysed expression of the same set of genes in the set of tumour cell primary cultures previously analysed for *Lyn* conditional allele recombination and *Lyn* gene and LYN protein expression (Fig. 3). In contrast to the results from the whole-tumour analysis, there were no significant differences between cultured cells, whether we compared cultures from different cohorts (Fig. 7C), cultures with different levels of *Lyn* gene expression (Fig. 7D) or cultures with different levels of LYN protein expression (Fig. 7E).

B-cell abundance in tumours correlates with doubling time

The results of the qRT-PCR validation suggest either that the differences in tumour biology indicated by the RNAseq analysis are not a result of differences between the neoplastic cells in the tumours but are a consequence of other cell types, or that differences only appear between the neoplastic cells when they are in the context of an *in vivo* microenvironment. A combination of the two factors is also possible.

One potential difference between the *Lyn*-low/PCA group 1/2 and *Lyn*-high/PCA group 3/4 tumours is the extent of immune cell infiltration. This possibility is supported by immunoglobulin genes being significantly more highly expressed in the *Lyn*-high/PCA group 3/4 tumours (Table S9), the enrichment of this tumour group for 'inflammation and immunity'-associated genes (Fig. 6) and the known high expression of *Lyn* in immune cell subsets, particularly in B cells (Brian and Freedman, 2021). Therefore, to assess the immune cell infiltration between the tumour groups, we analysed the RNAseq data using CIBERSORTx (Steen et al., 2020).

There were no significant differences in immune cell subsets between the tumour groups (Fig. S7; Table S13). However, when considering memory B cells and plasma cells in particular (two subsets likely to contribute significantly to a *Lyn*-high and high immunoglobulin gene expression signature), the *Lyn*-high/PCA group 3/4 tumours had a higher mean abundance of cells than the *Lyn*-low/PCA group 1/2 tumour group, but also with large error bars (memory B-cell abundance of *Lyn*-low tumours, 30.007 ±35.411, n=13; memory B-cell abundance of *Lyn*-high tumours, 126.619±119.442, n=13; plasma cell abundance of *Lyn*-low tumours, 1.614±2.689, n=13; plasma cell abundance of *Lyn*-high tumours, 41.141±51.980, n=13; mean±s.d.; two-tailed unpaired t-tests failed to meet the significance threshold following correction for multiple testing across the CIBERSORTx dataset) (Fig. S7; Table S13). Therefore, although a subset of *Lyn*-high/PCA group 3/4 tumours did have high levels of immune cells likely to contribute to tumour gene expression signatures, this was not true of all of them.

Lyn-high/PCA group 3/4 tumours had a higher histoscore than *Lyn*-low/PCA group 1/2 tumours (Figs 4D and 5C), so we next assessed whether there was an association between LYN staining of tumour cells, as assessed by histoscores, and B-cell abundance. The group of tumours with the highest histoscore included four tumours with the highest abundance of B cells. However, the tumours with high LYN tumour cell histoscores also included tumours with low or no B-cell infiltrate, and there was no significant difference in abundance overall among tumours with different levels of LYN staining (Fig. 8A,B).

Finally, we determined whether there was an association between B-cell abundance and tumour-doubling time. Indeed, there was a significant association between memory B-cell (P=0.0067) but not plasma cell (P=0.0935) abundance and tumour-doubling times (Fig. 8C).

DISCUSSION

The SRC-family kinase LYN is most highly expressed in haematopoietic cells but is also expressed in a wide variety of other tissues, including epithelia (reviewed in Brian and Freedman, 2021). It is a downstream target of c-KIT signalling in luminal epithelial stem/progenitor cells of the mammary gland (Regan et al., 2012; Tornillo et al., 2018) and also expressed in breast cancers, particularly TNBC (Choi et al., 2010; Hochgrafe et al., 2010; Molyneux et al., 2010).

The LYN kinase is best known for its role as both a positive and negative regulator of myeloid and B-cell development and differentiation (Brian and Freedman, 2021). The positive functions of LYN are context dependent and, in positive signalling, loss of LYN may be compensated for by other SRC-family kinases. In contrast, LYN appears to be absolutely required for negative regulation of B-cell proliferation (Brian and Freedman, 2021; Xu et al., 2005). Notably, both *Lyn* knockout mice and mice constitutively overexpressing LYN develop lethal autoimmune kidney diseases, although of distinct pathologies (Hibbs et al., 2002, 1995).

LYN has two splice isoforms (LYN^{FL}/LYN p56/LYNA and $LYN^{\Delta 25\text{-}45}$/LYN p53/LYNB) (Brian and Freedman, 2021; Tornillo et al., 2018; Xu et al., 2005), and a ΔNLYN caspase-cleaved variant that affects NFκB signalling has also been described (Marchetti et al., 2009). These splice isoforms are still not fully understood, although it is known that LYNA regulates a signalling checkpoint in macrophages (Freedman et al., 2015) and re-expression of either LYNA or LYNB in *Lyn* knockout mice restores B-cell developmental defects, but neither rescues the autoimmune phenotype on its own (Brian et al., 2022).

Previous studies on the mammary epithelium and breast cancer, including our own, have highlighted LYN as a positive regulator of cell growth and survival (Choi et al., 2010; Tornillo et al., 2018). We have shown that LYNA specifically regulates cell invasion and migration in TNBC cell lines *in vitro* but both LYNA and LYNB enhance breast cancer cell line survival, suggesting that *Lyn* is an oncogene (Tornillo et al., 2018). Tyrosine 32 in the LYNA-specific N-terminal region is a target of EGFR kinase activity and, once phosphorylated, results in LYN-mediated activation of the MCM7 DNA replication-licencing factor (Huang et al., 2013). LYN activity has been reported to promote the epithelial-mesenchymal transition through Vav-Rac1-PAK1-mediated control of SNAI protein localisation and stability in multiple cancer types, including breast cancer (Thaper et al., 2017). A role for LYN in the regulation of p53 has also been described. LYN is reported to directly interact with p53 and prevent its nuclear export, suppressing MDM2-mediated p53 degradation and enhancing p53-dependent apoptosis (Ren et al., 2002).

Here, we find contradictory evidence for the role of LYN in mammary tumours, potentially related to functions in multiple cell types within a tumour. LYN protein expression was decreased in epithelial-origin neoplastic tumour cells carrying two copies of a conditional knockout *Lyn* allele in which Cre recombinase expression was under the control of the *Blg* promoter (Fig. 3C).

Disease Models & Mechanisms (2024) 17, dmm050211. doi:10.1242/dmm.050211

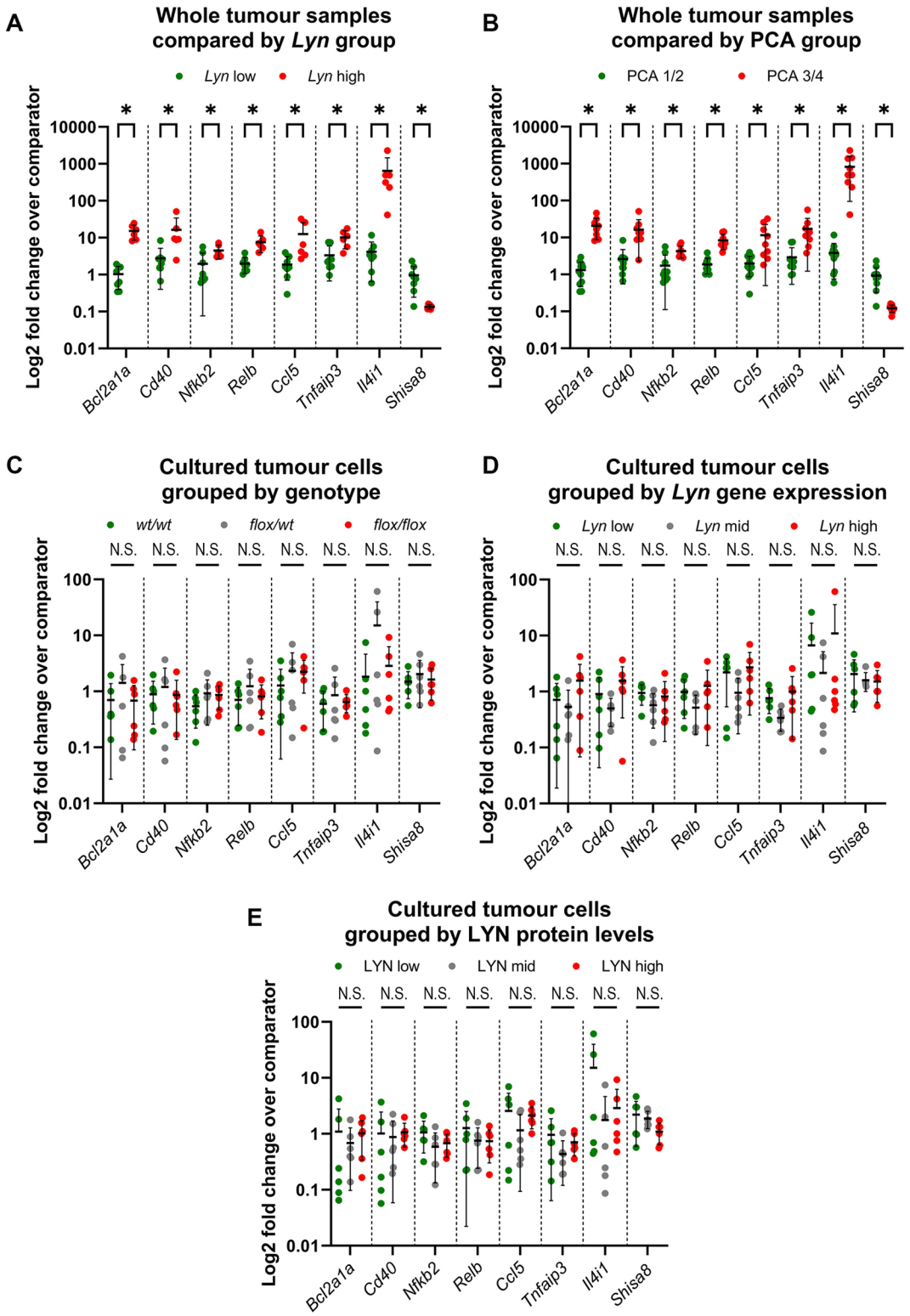

Fig. 7. Gene expression differences between tumours *in vivo* are not maintained in neoplastic tumour cells in primary culture. (A,B) qRT-PCR validation of *Ccl5*, *Tnfaip3*, *Bcl2a1a*, *Cd40*, *Nfkb2*, *Relb*, *Shisa8* and *Il4i1* expression in whole tumour samples analysed by RNAseq, comparing *Lyn*-low (n=8) and *Lyn*-high (n=6) (A) and PCA group 1/2 (n=11) and PCA group 3/4 (n=9) (B) tumour groups. Patterns of gene expression are consistent with the RNAseq data. (C-E) qRT-PCR expression of the same gene set in primary cultures of neoplastic tumour cells from $Lyn^{wt/wt}$, $Lyn^{fl/wt}$ and $Lyn^{fl/fl}$ tumours (n=6 of each genotype). Expression is compared by genotype (C), previously determined levels of *Lyn* gene expression (D) or previously determined levels of LYN protein expression (E) (Fig. 3). Cultures were divided into three groups based on high (top third), mid (middle third) or low (bottom third) levels of expression. There were no differences between any groups in the cultured cell analysis. Data are presented as expression levels normalised to *Gapdh* and *Actb* (A,B) or *Gapdh* alone (C,D) (Fig. S6) and relative to comparator samples (Table S12). For each gene, datasets are presented by sample group in the order shown in the legend underneath the graph title. Mean±s.d. is shown; Mann–Whitney tests with multiple comparison correction. N.S., not significant; *P<0.05.

Disease Models & Mechanisms (2024) 17, dmm050211. doi:10.1242/dmm.050211

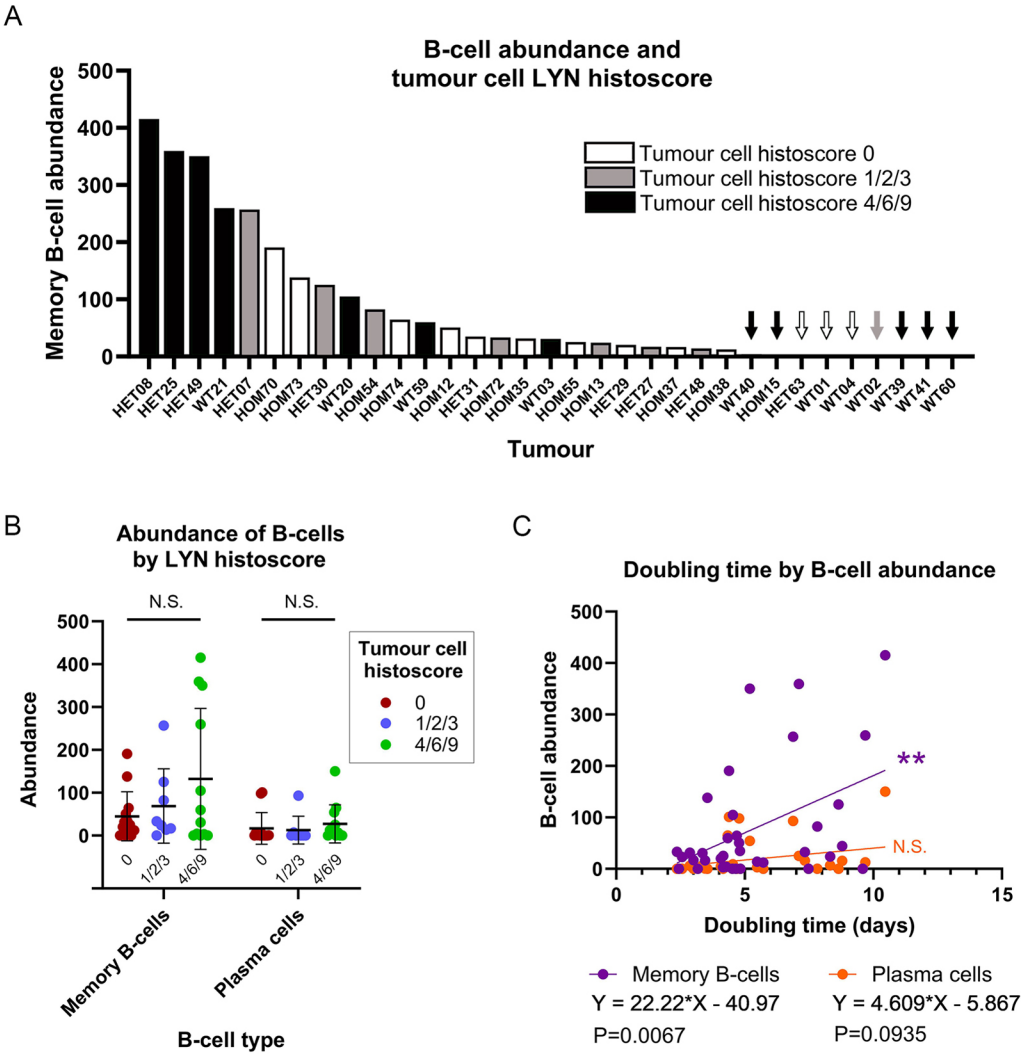

Fig. 8. Memory B-cell abundance correlates with tumour-doubling time. (A) Memory B-cell abundance in 33 RNAseq tumour samples plotted from highest to lowest abundance (arbitrary units) and colour-coded by tumour cell LYN histoscore for the tumour. Very low/zero abundance samples are indicated by colour-coded arrows. WT, wild-type tumours; HET, heterozygous tumours; HOM, homozygous tumours. (B) Memory B-cell and plasma cell abundance compared by tumour cell LYN histoscore groups (n=13, 8 and 12 for groups 0, 1/2/3 and 4/6/9, respectively). Mean±s.d. is shown. (two-way ANOVA). (C) Simple linear regression of B-cell abundance (arbitrary units) (memory B cell, purple; plasma cells, orange) against tumour-doubling time (days) (n=36). Increased numbers of memory B cells are significantly associated with increased tumour-doubling time. N.S., not significant; **P<0.01.

However, some tumours retained strong LYN expression, suggesting incomplete recombination *in vivo*; furthermore, some tumours with wild-type alleles showed very low levels of expression. Importantly, there was no association between LYN protein expression (assessed by histoscores) and tumour-doubling time (Fig. 4F).

In contrast, there was an association between *Lyn* expression levels as measured by RNAseq in whole-tumour lysates and tumour-doubling time (tumours with higher overall *Lyn* expression grew more slowly; Fig. 4E), and when tumours were grouped in an unsupervised manner on the basis of RNAseq data, there was also a correlation with doubling time (Fig. 5D). Therefore, overall *Lyn* expression correlated with tumour-doubling time, but LYN expression specifically in the tumour cells did not. Rather, tumour-doubling time correlated with B-cell abundance (as defined by CIBERSORTx, which has been previously proven to be robust) (Steen et al., 2020), with tumours with a higher B-cell abundance score growing more slowly (Fig. 8C); there tended to be more B cells in *Lyn*-high/PCA group 3/4 tumours, although with considerable variation (Fig. S7). As B cells are known to express *Lyn*, their presence in a tumour would tend to result in tumours with a heavy B-cell infiltration being grouped in the *Lyn*-high/PCA group 3/4 set (and in this tumour set having significantly higher levels of expression of ‘inflammation and immunity’-related genes).

As there was an association between tumour cell LYN histoscore and the *Lyn* tumour group defined by RNAseq analysis (Figs 4D and 5D), high *Lyn* expression in the whole-tumour lysates likely resulted from a combination of moderate or high levels of *Lyn* transcripts in the neoplastic tumour cells themselves as well as varying degrees of B-cell infiltrate, with very high abundance in some cases. It was the B-cell infiltrate that correlated with the doubling time of the tumours rather than levels of LYN expression in the tumour cells.

However, it is possible that LYN-dependent signalling pathways in tumour cells activated intrinsic inflammatory signalling pathways, potentially including NFκB, resulting in the production of cytokines that enhanced immune cell recruitment and an anti-tumour immune response. Downstream mediators linked to LYN activation of NFκB include MEK, IKKα (or CHUK) (Cooper et al., 2013), PI3K (Toubiana et al., 2015), MAPK and IκB (Avila et al., 2012), and there is also support for a role of NFκB activation in BRCA1 loss-of-function-associated breast cancers. NFκB activation was proposed to be the mechanism underlying hormone-independent growth of *BRCA1*-deficient luminal progenitors in colony formation assays *in vitro* (Lim et al., 2009; Sau et al., 2016). In contrast, a subset of *BRCA1*-mutant breast cancers was reported to show increased NFκB activity correlating with a good prognosis (Buckley et al., 2016). These tumours were associated with increased numbers of $CD8^+$ cytotoxic T cells, suggested to create an ‘anti-tumour

Disease Models & Mechanisms (2024) 17, dmm050211. doi:10.1242/dmm.050211

microenvironment' (Buckley et al., 2016). The difference between these *in vitro* and *in vivo* studies reflects our own findings.

Our study has limitations. In particular, LYN staining may not reflect active LYN protein or active LYN-dependent signalling. Unfortunately, antibodies specific for active phosphorylated LYN are not currently available for IHC. Those that are available stain the phosphorylated active site of all SRC-family kinases. Flow cytometry to purify neoplastic tumours cells for analysis by, for example, western blotting, is also problematic. Antibodies that can specifically mark all neoplastic epithelial-origin cells as opposed to non-neoplastic epithelia, or indeed other components of the tumour are not available. In the absence of a robust approach to purifying tumour cells, we opted to carry out RNAseq analysis from pieces of tumour that likely contained mixed populations of cells. Such pieces were taken from tumour regions away from obvious necrosis but without any other selection criteria. This has the advantage of ensuring that sensitive RNA expression patterns are not altered during cell purification protocols but, assuming that *Lyn* expression in *Lyn*-high tumours was a result of both LYN-expressing tumour cells and immune cells, interpretation of the results is complex. Future studies to test our model that the activity of LYN-dependent, cell-intrinsic signalling pathways results in an anti-tumour immune response will likely require single-cell transcriptomic analysis or a similar approach.

Overall, our study suggests that, despite previous evidence supporting a cell-intrinsic role for LYN kinase in promoting mammary tumour cell survival, proliferation and invasion, it is likely to present difficulties as a therapeutic target in breast cancer owing to its potential role in B cells and the anti-tumour immune response. We also suggest that previous studies reporting associations between *Lyn* overexpression in TNBC may actually be reflecting enrichment in TNBC for immune cells, as is being exploited by current immunotherapy trials in this setting (Tarantino et al., 2022).

MATERIALS AND METHODS

See Table S1 for a full list of all primers, antibodies and other reagents. Raw scanned western blots are provided in Fig. S8.

Establishment of genetically modified mouse lines

This study was approved by the Cardiff University Animal Welfare and Ethical Review Body and carried out under the authority of appropriate Home Office Personal and Project Licences and with reference to ARRIVE guidelines (Percie du Sert et al., 2020). In particular, animals were monitored regularly and predefined humane endpoints strictly adhered to. The numbers of animals required in each cohort were based on previous experience of requirements for a sufficiently powered tumour cohort study (typically 15-20 animals per cohort depending on effect size, but given the inherent random nature of litter sizes, sex ratios and genotypes, numbers in each cohort may not be identical). Randomisation was not appropriate as animals had to be assigned to cohorts according to their genotype. Only female animals were used.

The full breeding scheme is illustrated in Fig. S1. Mice carrying the conditional *Brca1* allele on the *p53* heterozygote background as well as a Cre recombinase under the control of the β-lactoglobulin mammary specific promoter (*BlgCre Brca1*$^{fl/fl}$ *p53*$^{+/-}$ mice) have been previously described (McCarthy et al., 2007; Molyneux et al., 2010). Mice carrying a tamoxifen-activated Cre ubiquitously expressed from the *Rosa26* locus (*R26C*) (Hameyer et al., 2007) were obtained from Prof. Karen Blyth, Cancer Research UK Beatson Centre, Glasgow. Mice carrying the *Lyn* floxed exon 4 conditional allele (*Lyn*^{tm1c}) were obtained from the Mary Lyon Centre, MRC Harwell (full nomenclature C57BL/6N-Lyn$^{tm1c(EUCOMM)Hmgu}$/H, derived from the embryonic stem cell clone HEPD0704_6_B11). Full details of all animals used in the study and all histological samples are provided in Tables S2 and S3.

Mouse mammary epithelial cell harvest and culture

Mammary epithelial organoids were prepared from fourth mammary fat pads of 10- to 12-week-old virgin female mice as described (Smalley, 2010). Intramammary lymph nodes were removed prior to tissue collection. Fat pads were finely minced on a McIlwain Tissue Chopper (Thermo Fisher Scientific) and then digested for 1 h at 37°C in 3 mg/ml collagenase A (Merck Sigma-Aldrich)/1.5 mg/ml trypsin (Merck Sigma-Aldrich) in serum- and Phenol Red-free L15 medium (Thermo Fisher Scientific/Invitrogen) with gentle rotation. Tissue fragments ('organoids') released were incubated for 5 min in Red Blood Cell Lysis buffer (Merck Sigma-Aldrich), washed and then plated for 1 h at 37°C in Dulbecco's modified Eagle medium (DMEM; Thermo Fisher Scientific/Invitrogen) containing 10% fetal bovine serum (FBS; Thermo Fisher Scientific) for depletion of fibroblasts by differential attachment.

For 3D cultures, organoids were incubated with 0.05% trypsin/EDTA (Thermo Fisher Scientific) for 2 min at 37°C prior to plating onto Growth Factor Reduced Phenol Red-free Matrigel (Thermo Fisher Scientific) in complete growth medium [DMEM/F12 (Thermo Fisher Scientific) with 10% charcoal-stripped FBS (Thermo Fisher Scientific), 5 µg/ml insulin (Merck Sigma-Aldrich), 10 ng/ml cholera toxin (Merck Sigma-Aldrich) and 10 ng/ml epidermal growth factor (Merck Sigma-Aldrich). 4-Hydroxytamoxifen (4OHT) (Merck Sigma-Aldrich) was added at a final concentration 100 nM for 10-12 h to induce the recombination of the *Lyn*^{fl} allele.

Isolation of primary tumour cells

Primary tumour epithelial cells were obtained using the gentleMACS Dissociator and Mouse Tumor dissociation kit (Miltenyi Biotec) following the protocol recommended for dissociation of tough tumours. To ensure efficient dissociation, volumes of enzyme D, enzyme R and enzyme A were scaled up according to the size of the tumour piece (100, 50 and 12.5 µl, respectively, per each 0.5 cm^3). The optional red blood cell lysis step was included in the procedure. Resulting cells were plated in complete growth medium in two-dimensional (2D) adherent conditions. Cells at passage 0 were used for all the experiments in this study.

Tumour measurements and doubling times

Tumour width (W) and length (L) were measured using a caliper twice a week by the same person each time to eliminate inter-operator variability. Volume was calculated using the formula $L \times W^2/2$.

IHC and formalin-fixed paraffin-embedded sample processing

Mice were euthanised by an approved method when previously established humane endpoints were reached. A full necropsy was performed and any tumour tissue was fixed in 10% neutral-buffered formalin for 24 h at 4°C, before being processed into paraffin blocks according to standard procedures. When a tumour was of sufficient size, a piece (distant from any obvious necrosis) was also snap frozen on dry ice at the time of dissection and then stored at −80°C for later RNA/protein extraction. In some cases, pieces of tumour were kept in L15 medium on ice for later isolation and culture of primary tumour cells. Visceral organs (liver, kidneys, spleen, lungs and, in some cases, heart and stomach, if obvious pathology was present) were also fixed in neutral-buffered formalin for 24 h and processed into paraffin blocks.

Tissue sections (5 µm) were either stained using Haematoxylin and Eosin (H&E) for histological analysis or used for immunohistochemical staining. For the latter, freshly cut sections were dewaxed and rehydrated. Sections underwent antigen retrieval in citrate buffer, pH 6.0, in a pressure cooker for 15 min before incubation with a 3% hydrogen peroxide solution for 20 min and then blocking in TBS containing 10% goat serum and 0.1% Tween-20 for 1 h. Incubation with primary antibodies (Table S1) was performed overnight at 4°C. Detection was carried out using the ImmPRESS kit (Vector Labs). Sections were counterstained with Haematoxylin and mounted. Images were acquired using a VS200 slide scanner (Olympus Keymed, Southend-on-Sea, Essex, UK) with a 20× objective and visualised using OlyVIA slide viewer software (Olympus).

Disease Models & Mechanisms (2024) 17, dmm050211. doi:10.1242/dmm.050211

Histopathological analysis

Mammary tumour phenotyping was carried out by M.J.S. (who has over 10 years of experience of using the four-histotype classification system for mouse mammary tumours) using our previously established criteria based primarily on morphology of H&E-stained sections and immunohistochemical staining for ΔNp63 (Melchor et al., 2014; Molyneux et al., 2010; Ordonez et al., 2023, 2019, 2021). In brief, assessment of metaplasia (either spindle cell or squamous) and the extent of any ΔNp63 staining allows mouse mammary epithelial tumours to be classified as adenosquamous tumours (extensive squamous metaplasia and abundant ΔNp63 staining), adenomyoepitheliomas (abundant ΔNp63 staining in a distinct pseudobasal pattern bordering ΔNp63-negative cells, but little or no metaplasia), metaplastic spindle cell carcinomas (extensive or near total spindle cell metaplasia with infrequent nests of epithelial tumour cells; no ΔNp63 staining), adenocarcinomas of no special type (little or no metaplasia and little ΔNp63 staining). Histology of other organs was reviewed by M.J.S. with support and advice from S.B.

Scoring of Ki67 IHC

For Ki67 IHC quantification, images of five different regions (in one case, six regions) from each section were captured using the OlyVIA software at 10× magnification. Regions were chosen to include areas with the highest level of Ki67 staining for that section, so that the final score represented the highest potential for proliferation, and therefore the most aggressive behaviour, of that tumour. The percentage of positive tumour cells in each image was determined automatically using Cognition Master Professional Ki67 Quantifier (Medline Scientific, Chalgrove, Oxfordshire, UK). Values returned by the program were 'sense-checked' against each image; any obvious errors (e.g. autopsy number 21-34-03, field 5, Table S4) were excluded from further analysis.

Scoring of LYN IHC staining by modified histoscore

LYN IHC staining using a rabbit polyclonal antibody (Thermo Fisher Scientific) was quantified by a modified histoscore approach considering strength of staining and area stained. If staining was visible at 0.2× magnification on the OlyVIA slide viewer images, it was scored as strength '3'. If staining was not visible at 0.2× but was visible at 2×, it was scored as strength '2'. If staining was not visible at 2× but was visible at 20×, it was scored as strength '1'. If no staining was visible at 20×, it was scored as '0'. For the area of tumour stained, scoring was determined as follows: 0, no staining; 1, <10% of tumour cells positive; 2, 10-50% of tumour cells positive; 3, >50% of tumour cells positive. These divisions were chosen as easily assessable by eye, without the need for exact counting. The two scores were then multiplied together to give a final value. Note that the antibody used measured total LYN protein, not active protein. Antibodies specific to the phosphorylation site on LYN that indicate activation are not currently available.

Protein isolation and western blotting analysis

2D cultured cells were lysed in Laemmli buffer. 3D cultured primary mouse mammary cells were released from Matrigel using the BD cell recovery solution (Corning/Thermo Fisher Scientific) prior to lysis. Protein extracts were separated by SDS-PAGE on 4-15% gradient Mini-PROTEAN TGX Precast Protein Gels (Bio-Rad), transferred to PVDF membranes (IPVH00010, Merck Millipore) and immunoblotted with anti-LYN antibodies. GAPDH was used as the loading control. The resulting immunocomplexes were detected by HRP-conjugated anti-mouse IgG or anti-rabbit IgG secondary antibodies and enhanced chemiluminescent (ECL) reagents (WBLUF0100, Merck Millipore).

RNA isolation and gene expression analysis

Total RNA was isolated from tumour tissue or 2D cultured cells using the RNeasy Minikit (QIAGEN) according to the manufacturer's protocol. TRIzol (Thermo Fisher Scientific) was used for RNA extraction from 3D cultured primary mammary organoids. Up to 1 µg of RNA was converted into cDNA using either the Quantitect Reverse Transcription kit (QIAGEN) or the Superscript IV transcription kit (Thermo Fisher Scientific) following the manufacturer's instructions. Gene expression analysis was carried out using either TaqMan Master Mix and Taqman gene expression assays (Thermo Fisher Scientific) or Applied Biosystems SYBR Green Master Mix (Thermo Fisher Scientific), and primers were designed using Primer3 V4.1.0 (https://primer3.ut.ee/) (Table S1). Data analysis was carried out using the QuantStudio 7 software (Thermo Fisher Scientific). Relative expression levels of target genes were calculated using the ΔΔCt method as described previously (Kendrick et al., 2008).

For validation of RNAseq analysis of whole tumours, the geometric mean of *Gapdh* and *Actb* Ct values was used as a reference (Vandesompele et al., 2002). However, for analysis of passage 0 tumour cells in culture, only *Gapdh* was used as the reference, as analysis of *Actb* variance in these cells suggested a batch effect, which may have confounded the results (Fig. S6).

RNA sequencing and analysis

Samples for RNAseq analysis underwent an on-column DNase I digestion step for genomic DNA removal prior to further processing. Total RNA quality and quantity was assessed using Agilent 4200 TapeStation and RNA or high-sensitivity RNA ScreenTapes (Agilent Technologies). mRNA was isolated from 50 ng of total RNA (RNA integrity number >7) using the NEBNext Poly(A) mRNA magnetic isolation module [New England Biolabs (NEB), E7490] and the sequencing libraries were prepared using the NEB Ultra II Directional RNA Library Prep Kit for Illumina (NEB, E7760). The sequencing libraries were prepared following Chapter 1 of the protocol in this kit. The steps included mRNA isolation, fragmentation and priming, first-strand cDNA synthesis, second-strand cDNA synthesis, adenylation of 3′ ends, adapter ligation (1:80 dilution) and PCR amplification (14 cycles). Libraries were validated using the Agilent 4200 TapeStation and hsD1000 ScreenTapes (Agilent Technologies) to ascertain the insert size, and a Qubit fluorometer (Thermo Fisher Scientific) was used to perform fluorometric quantitation. The manufacturer's instructions were followed except for the replacement of SPRIselect Beads or NEBNext Sample Purification Beads by AMPure XP beads (Beckman Coulter) in purification steps. The validated libraries were normalized to 4 nM, pooled together and the pool sequenced on an S1 (200-cycle) flow cell using a 2×100 bp dual-index format on the Illumina NovaSeq6000 sequencing system according to the manufacturer's instructions. Samples were sequenced to a read depth of at least 35 million prior to quality trimming with fastp (Chen et al., 2018). Quality trimmed reads were mapped to GRCm38 using STAR (v2.5.1b) (Dobin and Gingeras, 2015) with read multimapping filter set to 1 and gtf Gencode GRCm38 vM17. Exon and gene counts were calculated with featureCounts (v1.5.1) (Liao et al., 2014). Differential gene expression was calculated with SARtools using the DESeq2 package (Varet et al., 2016).

GSEA

For GSEA, significant DEGS from the different tumour groups [adjusted *P*-value <0.05; $\log_2$(fold change) <0.5 or >2.0] were uploaded to g:Profiler (https://biit.cs.ut.ee/gprofiler/gost) and queried against the *Mus musculus* database with a term size limit of 1000, but otherwise using default options (with the exception of one group: the DEGs overlapping between the PCA group 1/2 and *Lyn*-low tumour groups, for which the term size limit was allowed default values, otherwise no results were returned). Results were downloaded as a CSV file (default options). GO BP grouping into functional categories was carried out manually.

CIBERSORTx analysis (https://cibersortx.stanford.edu/) (Newman et al., 2019) was carried out using the LM22 signature matrix file for 22 immune cell types and was run in 'absolute mode' so that relative differences between the proportions of immune cell types would be maintained.

Statistics

All statistical analysis was carried out in Prism 10.0.2 (GraphPad Software). Survival curves were analysed by log rank test. For all other experiments, normally distributed data were analysed by Brown–Forsythe two-way ANOVA and/or two-tailed unpaired *t*-tests where appropriate. Non-parametric data were analysed by Kruskel–Wallis and/or Mann–Whitney tests where appropriate. A *P*-value of <0.05 was taken as significant. For analysis of difference in distribution of categorical variables, χ^2 test (two

groups) or χ^2 test for trend (more than two groups) was used. *P*-values from multiple testing were corrected using the Holm–Sidak method.

The numbers of tumours available for analysis varied depending on the assay – for some tumours, doubling data were not available (as a minimum of three measurements was needed to determine this), and for others, IHC analysis was not available due to e.g. technical failures or poor quality/quantity of embedded material. For the RNAseq analysis, group sizes for determining DEGs varied depending on whether analyses were supervised or unsupervised. *n*-values numbers are provided in the figure legends.

Acknowledgements
We acknowledge our colleagues at Wales Gene Park for their insight and expertise that assisted this research, and for their technical and bioinformatic support in generating and analysing the next-generation sequencing data. Wales Gene Park is an infrastructure support group with funding from Welsh Government through Health and Care Research Wales. The authors would like to thank the Freedman laboratory and also Catherine Hogan for their comments on the manuscript.

Competing interests
The authors declare no competing or financial interests.

Author contributions
Conceptualization: G.T., M.J.S.; Formal analysis: G.T., L.W., H.K., A.T.H., T.H., S.B., M.J.S.; Investigation: G.T., L.W., H.K., A.T.H., T.H., S.B., M.J.S.; Writing - original draft: G.T., M.J.S.; Supervision: M.J.S.; Project administration: M.J.S.; Funding acquisition: G.T., M.J.S.

Funding
This work was supported by Breast Cancer Now (2018NovPR1211). The RNAseq work was supported by Breast Cancer Research Aid. Open Access funding provided by Cardiff University. Deposited in PMC for immediate release.

Data availability
RNAseq data have been deposited at the Gene Expression Omnibus (GEO) with the accession number GSE222075.

References
Avila, M., Martinez-Juarez, A., Ibarra-Sanchez, A. and Gonzalez-Espinosa, C. (2012). Lyn kinase controls TLR4-dependent IKK and MAPK activation modulating the activity of TRAF-6/TAK-1 protein complex in mast cells. *Innate. Immun.* **18**, 648-660. doi:10.1177/1753425911435265

Brian, B. F. and Freedman, T. S. (2021). The Src-family kinase Lyn in immunoreceptor signaling. *Endocrinology* **162**, bqab152. doi:10.1210/endocr/bqab152

Brian, B. F. T., Sauer, M. L., Greene, J. T., Senevirathne, S. E., Lindstedt, A. J., Funk, O. L., Ruis, B. L., Ramirez, L. A., Auger, J. L., Swanson, W. L. et al. (2022). A dominant function of LynB kinase in preventing autoimmunity. *Sci. Adv.* **8**, eabj5227. doi:10.1126/sciadv.abj5227

Buckley, N. E., Haddock, P., De Matos Simoes, R., Parkes, E., Irwin, G., Emmert-Streib, F., McQuaid, S., Kennedy, R. and Mullan, P. (2016). A BRCA1 deficient, NFκB driven immune signal predicts good outcome in triple negative breast cancer. *Oncotarget* **7**, 19884-19896. doi:10.18632/oncotarget.7865

Chen, S., Zhou, Y., Chen, Y. and Gu, J. (2018). fastp: an ultra-fast all-in-one FASTQ preprocessor. *Bioinformatics* **34**, i884-i890. doi:10.1093/bioinformatics/bty560

Choi, Y. L., Bocanegra, M., Kwon, M. J., Shin, Y. K., Nam, S. J., Yang, J. H., Kao, J., Godwin, A. K. and Pollack, J. R. (2010). LYN is a mediator of epithelial-mesenchymal transition and a target of dasatinib in breast cancer. *Cancer Res.* **70**, 2296-2306. doi:10.1158/0008-5472.CAN-09-3141

Cooper, M. J., Cox, N. J., Zimmerman, E. I., Dewar, B. J., Duncan, J. S., Whittle, M. C., Nguyen, T. A., Jones, L. S., Ghose Roy, S., Smalley, D. M. et al. (2013). Application of multiplexed kinase inhibitor beads to study kinome adaptations in drug-resistant leukemia. *PLoS One* **8**, e66755. doi:10.1371/journal.pone.0066755

Croucher, D. R., Hochgrafe, F., Zhang, L., Liu, L., Lyons, R. J., Rickwood, D., Tactacan, C. M., Browne, B. C., Ali, N., Chan, H. et al. (2013). Involvement of Lyn and the atypical kinase SgK269/PEAK1 in a basal breast cancer signaling pathway. *Cancer Res.* **73**, 1969-1980. doi:10.1158/0008-5472.CAN-12-1472

Densham, R. M. and Morris, J. R. (2017). The BRCA1 Ubiquitin ligase function sets a new trend for remodelling in DNA repair. *Nucleus* **8**, 116-125. doi:10.1080/19491034.2016.1267092

Dobin, A. and Gingeras, T. R. (2015). Mapping RNA-seq reads with STAR. *Curr. Protoc. Bioinformatics* **51**, 11 14 1-11 14 19. doi:10.1002/0471250953.bi1114s51

Foo, T. K. and Xia, B. (2022). BRCA1-dependent and independent recruitment of PALB2-BRCA2-RAD51 in the DNA damage response and cancer. *Cancer Res.* **82**, 3191-3197. doi:10.1158/0008-5472.CAN-22-1535

Freedman, T. S., Tan, Y. X., Skrzypczynska, K. M., Manz, B. N., Sjaastad, F. V., Goodridge, H. S., Lowell, C. A. and Weiss, A. (2015). LynA regulates an inflammation-sensitive signaling checkpoint in macrophages. *Elife* **4**, 2002823. doi:10.1183/13993003.02823-2020

Fu, X., Tan, W., Song, Q., Pei, H. and Li, J. (2022). BRCA1 and breast cancer: molecular mechanisms and therapeutic strategies. *Front. Cell Dev. Biol.* **10**, 813457. doi:10.3389/fcell.2022.813457

Hameyer, D., Loonstra, A., Eshkind, L., Schmitt, S., Antunes, C., Groen, A., Bindels, E., Jonkers, J., Krimpenfort, P., Meuwissen, R. et al. (2007). Toxicity of ligand-dependent Cre recombinases and generation of a conditional Cre deleter mouse allowing mosaic recombination in peripheral tissues. *Physiol. Genomics* **31**, 32-41. doi:10.1152/physiolgenomics.00019.2007

Hibbs, M. L., Tarlinton, D. M., Armes, J., Grail, D., Hodgson, G., Maglitto, R., Stacker, S. A. and Dunn, A. R. (1995). Multiple defects in the immune system of Lyn-deficient mice, culminating in autoimmune disease. *Cell* **83**, 301-311. doi:10.1016/0092-8674(95)90171-X

Hibbs, M. L., Harder, K. W., Armes, J., Kountouri, N., Quilici, C., Casagranda, F., Dunn, A. R. and Tarlinton, D. M. (2002). Sustained activation of Lyn tyrosine kinase in vivo leads to autoimmunity. *J. Exp. Med.* **196**, 1593-1604. doi:10.1084/jem.20020515

Hochgrafe, F., Zhang, L., O'Toole, S. A., Browne, B. C., Pinese, M., Porta Cubas, A., Lehrbach, G. M., Croucher, D. R., Rickwood, D., Boulghourjian, A. et al. (2010). Tyrosine phosphorylation profiling reveals the signaling network characteristics of Basal breast cancer cells. *Cancer Res.* **70**, 9391-9401. doi:10.1158/0008-5472.CAN-10-0911

Huang, T. H., Huo, L., Wang, Y. N., Xia, W., Wei, Y., Chang, S. S., Chang, W. C., Fang, Y. F., Chen, C. T., Lang, J. Y. et al. (2013). Epidermal growth factor receptor potentiates MCM7-mediated DNA replication through tyrosine phosphorylation of Lyn kinase in human cancers. *Cancer Cell* **23**, 796-810. doi:10.1016/j.ccr.2013.04.027

Kendrick, H., Regan, J. L., Magnay, F. A., Grigoriadis, A., Mitsopoulos, C., Zvelebil, M. and Smalley, M. J. (2008). Transcriptome analysis of mammary epithelial subpopulations identifies novel determinants of lineage commitment and cell fate. *BMC Genomics* **9**, 591. doi:10.1186/1471-2164-9-591

Kim, M. C., Choi, J. E., Lee, S. J. and Bae, Y. K. (2016). Coexistent loss of the expressions of BRCA1 and p53 predicts poor prognosis in triple-negative breast cancer. *Ann. Surg. Oncol.* **23**, 3524-3530. doi:10.1245/s10434-016-5307-z

Kuchenbaecker, K. B., Hopper, J. L., Barnes, D. R., Phillips, K. A., Mooij, T. M., Roos-Blom, M. J., Jervis, S., van Leeuwen, F. E., Milne, R. L., Andrieu, N. et al. (2017). Risks of breast, ovarian, and contralateral breast cancer for BRCA1 and BRCA2 mutation carriers. *JAMA* **317**, 2402-2416. doi:10.1001/jama.2017.7112

Liao, Y., Smyth, G. K. and Shi, W. (2014). featureCounts: an efficient general purpose program for assigning sequence reads to genomic features. *Bioinformatics* **30**, 923-930. doi:10.1093/bioinformatics/btt656

Lim, E., Vaillant, F., Wu, D., Forrest, N. C., Pal, B., Hart, A. H., Asselin-Labat, M. L., Gyorki, D. E., Ward, T., Partanen, A. et al. (2009). Aberrant luminal progenitors as the candidate target population for basal tumor development in BRCA1 mutation carriers. *Nat. Med.* **15**, 907-913. doi:10.1038/nm.2000

Liu, X., Holstege, H., van der Gulden, H., Treur-Mulder, M., Zevenhoven, J., Velds, A., Kerkhoven, R. M., van Vliet, M. H., Wessels, L. F., Peterse, J. L. et al. (2007). Somatic loss of BRCA1 and p53 in mice induces mammary tumors with features of human BRCA1-mutated basal-like breast cancer. *Proc. Natl. Acad. Sci. USA* **104**, 12111-12116. doi:10.1073/pnas.0702969104

Mahdavi, M., Nassiri, M., Kooshyar, M. M., Vakili-Azghandi, M., Avan, A., Sandry, R., Pillai, S., Lam, A. K. and Gopalan, V. (2019). Hereditary breast cancer; Genetic penetrance and current status with BRCA. *J. Cell. Physiol.* **234**, 5741-5750. doi:10.1002/jcp.27464

Marchetti, S., Gamas, P., Belhacene, N., Grosso, S., Pradelli, L. A., Colosetti, P., Johansen, C., Iversen, L., Deckert, M., Luciano, F. et al. (2009). The caspase-cleaved form of LYN mediates a psoriasis-like inflammatory syndrome in mice. *EMBO J.* **28**, 2449-2460. doi:10.1038/emboj.2009.183

Mateo, J., Lord, C. J., Serra, V., Tutt, A., Balmana, J., Castroviejo-Bermejo, M., Cruz, C., Oaknin, A., Kaye, S. B. and de Bono, J. S. (2019). A decade of clinical development of PARP inhibitors in perspective. *Ann. Oncol.* **30**, 1437-1447. doi:10.1093/annonc/mdz192

McCarthy, A., Savage, K., Gabriel, A., Naceur, C., Reis-Filho, J. S. and Ashworth, A. (2007). A mouse model of basal-like breast carcinoma with metaplastic elements. *J. Pathol.* **211**, 389-398. doi:10.1002/path.2124

Melchor, L., Molyneux, G., Mackay, A., Magnay, F. A., Atienza, M., Kendrick, H., Nava-Rodrigues, D., Lopez-Garcia, M. A., Milanezi, F., Greenow, K. et al. (2014). Identification of cellular and genetic drivers of breast cancer heterogeneity in genetically engineered mouse tumour models. *J. Pathol.* **233**, 124-137. doi:10.1002/path.4345

Molyneux, G., Geyer, F. C., Magnay, F. A., McCarthy, A., Kendrick, H., Natrajan, R., Mackay, A., Grigoriadis, A., Tutt, A., Ashworth, A. et al. (2010). BRCA1 basal-like breast cancers originate from luminal epithelial progenitors and not from basal stem cells. *Cell Stem Cell* **7**, 403-417. doi:10.1016/j.stem.2010.07.010

Newman, A. M., Steen, C. B., Liu, C. L., Gentles, A. J., Chaudhuri, A. A., Scherer, F., Khodadoust, M. S., Esfahani, M. S., Luca, B. A., Steiner, D. et al. (2019). Determining cell type abundance and expression from bulk tissues with digital cytometry. *Nat. Biotechnol.* **37**, 773-782. doi:10.1038/s41587-019-0114-2

Nolan, E., Lindeman, G. J. and Visvader, J. E. (2017). Out-RANKing BRCA1 in mutation carriers. *Cancer Res.* **77**, 595-600. doi:10.1158/0008-5472.CAN-16-2025

O'Donovan, P. J. and Livingston, D. M. (2010). BRCA1 and BRCA2: breast/ovarian cancer susceptibility gene products and participants in DNA double-strand break repair. *Carcinogenesis* **31**, 961-967. doi:10.1093/carcin/bgq069

Ordonez, L. D., Hay, T., McEwen, R., Polanska, U. M., Hughes, A., Delpuech, O., Cadogan, E., Powell, S., Dry, J., Tornillo, G. et al. (2019). Rapid activation of epithelial-mesenchymal transition drives PARP inhibitor resistance in Brca2-mutant mammary tumours. *Oncotarget* **10**, 2586-2606. doi:10.18632/oncotarget.26830

Ordonez, L. D., Melchor, L., Greenow, K. R., Kendrick, H., Tornillo, G., Bradford, J., Giles, P. and Smalley, M. J. (2021). Reproductive history determines Erbb2 locus amplification, WNT signalling and tumour phenotype in a murine breast cancer model. *Dis. Model. Mech.* **14**, dmm048736. doi:10.1242/dmm.048736

Ordonez, L., Tornillo, G., Kendrick, H., Hay, T. and Smalley, M. J. (2023). NOTCH and AKT signalling interact to drive mammary tumour heterogeneity. *Cancers (Basel)* **15**, 4324. doi:10.3390/cancers15174324

Percie du Sert, N., Hurst, V., Ahluwalia, A., Alam, S., Avey, M. T., Baker, M., Browne, W. J., Clark, A., Cuthill, I. C., Dirnagl, U. et al. (2020). The ARRIVE guidelines 2.0: updated guidelines for reporting animal research. *Br. J. Pharmacol.* **177**, 3617-3624. doi:10.1111/bph.15193

Regan, J. L., Kendrick, H., Magnay, F. A., Vafaizadeh, V., Groner, B. and Smalley, M. J. (2012). c-Kit is required for growth and survival of the cells of origin of Brca1-mutation-associated breast cancer. *Oncogene* **31**, 869-883. doi:10.1038/onc.2011.289

Ren, X., Cao, C., Zhu, L., Yoshida, K., Kharbanda, S., Weichselbaum, R. and Kufe, D. (2002). Lyn tyrosine kinase inhibits nuclear export of the p53 tumor suppressor. *Cancer Biol. Ther.* **1**, 703-708. doi:10.4161/cbt.323

Sau, A., Lau, R., Cabrita, M. A., Nolan, E., Crooks, P. A., Visvader, J. E. and Pratt, M. A. (2016). Persistent activation of NF-κB in BRCA1-deficient mammary progenitors drives aberrant proliferation and accumulation of DNA damage. *Cell Stem Cell* **19**, 52-65. doi:10.1016/j.stem.2016.05.003

Smalley, M. J. (2010). Isolation, culture and analysis of mouse mammary epithelial cells. *Methods Mol. Biol.* **633**, 139-170. doi:10.1007/978-1-59745-019-5_11

Steen, C. B., Liu, C. L., Alizadeh, A. A. and Newman, A. M. (2020). Profiling cell type abundance and expression in bulk tissues with CIBERSORTx. *Methods Mol. Biol.* **2117**, 135-157. doi:10.1007/978-1-0716-0301-7_7

Tarantino, P., Corti, C., Schmid, P., Cortes, J., Mittendorf, E. A., Rugo, H., Tolaney, S. M., Bianchini, G., Andre, F. and Curigliano, G. (2022). Immunotherapy for early triple negative breast cancer: research agenda for the next decade. *NPJ Breast Cancer* **8**, 23. doi:10.1038/s41523-022-00386-1

Thaper, D., Vahid, S., Nip, K. M., Moskalev, I., Shan, X., Frees, S., Roberts, M. E., Ketola, K., Harder, K. W., Gregory-Evans, C. et al. (2017). Targeting Lyn regulates Snail family shuttling and inhibits metastasis. *Oncogene* **36**, 3964-3975. doi:10.1038/onc.2017.5

Tornillo, G., Knowlson, C., Kendrick, H., Cooke, J., Mirza, H., Aurrekoetxea-Rodriguez, I., Vivanco, M. D. M., Buckley, N. E., Grigoriadis, A. and Smalley, M. J. (2018). Dual mechanisms of LYN kinase dysregulation drive aggressive behavior in breast cancer cells. *Cell Rep.* **25**, 3674-3692.e10. doi:10.1016/j.celrep.2018.11.103

Toubiana, J., Rossi, A. L., Belaidouni, N., Grimaldi, D., Pene, F., Chafey, P., Comba, B., Camoin, L., Bismuth, G., Claessens, Y. E. et al. (2015). Src-family-tyrosine kinase Lyn is critical for TLR2-mediated NF-κB activation through the PI 3-kinase signaling pathway. *Innate Immun.* **21**, 685-697. doi:10.1177/1753425915586075

Vandesompele, J., De Preter, K., Pattyn, F., Poppe, B., Van Roy, N., De Paepe, A. and Speleman, F. (2002). Accurate normalization of real-time quantitative RT-PCR data by geometric averaging of multiple internal control genes. *Genome Biol.* **3**, RESEARCH0034. doi:10.1186/gb-2002-3-7-research0034

Varet, H., Brillet-Gueguen, L., Coppee, J. Y. and Dillies, M. A. (2016). SARTools: a DESeq2- and EdgeR-based R pipeline for comprehensive differential analysis of RNA-seq data. *PLoS One* **11**, e0157022. doi:10.1371/journal.pone.0157022

Xu, Y., Harder, K. W., Huntington, N. D., Hibbs, M. L. and Tarlinton, D. M. (2005). Lyn tyrosine kinase: accentuating the positive and the negative. *Immunity* **22**, 9-18. doi:10.1016/j.immuni.2004.12.004

Yoshida, K. and Miki, Y. (2004). Role of BRCA1 and BRCA2 as regulators of DNA repair, transcription, and cell cycle in response to DNA damage. *Cancer Sci.* **95**, 866-871. doi:10.1111/j.1349-7006.2004.tb02195.x

Zhu, L., Pan, J. N., Qian, Z., Ye, W. W., Wang, X. J. and Cao, W. M. (2022). High chromosome instability identified by low-pass whole-genome sequencing assay is associated with TP53 copy loss and worse prognosis in BRCA1 germline mutation breast cancer. *Breast Cancer* **29**, 103-113. doi:10.1007/s12282-021-01286-1